



Review Article

## Room-Temperature Spin-Transition Iron Compounds

Nayathuparambil Thomas Madhu<sup>1,2\*</sup>, Esther Theresa Knittl<sup>4</sup>, Tegene Desalegn Zeleke<sup>3</sup>, Alemu Gonfa Robi<sup>2</sup> and Wolfgang Linert<sup>4\*</sup>

### Abstract

Spin transition complexes are an interesting class of materials exhibiting molecular bistability with potential applications in nanotechnological devices as memory storage units, sensors or displays. Since the discovery of the spin transition phenomenon in tris(N,N-dialkylthiocarbamato)iron(III) complexes, numerous investigations have been devoted to this field of molecular magnetism. The spin transition phenomenon is probably the most spectacular example of bistability in molecular chemistry. However, it is a challenge to obtain spin transition materials when working under ambient conditions (eg. room temperature and pressure), which would be highly advantageous for potential applications. So far, only some Fe(II) and Fe(III) molecular systems have shown temperature-induced spin transitions around and even above room temperature. Within this review, we discuss the characteristics of this class of bistable compounds in detail and we try to draw more general conclusions regarding the integration, implementation and application of spin transition compounds as switching elements in hybrid molecular devices.

### Keywords

Iron complexes; Spin transition; Room temperature; Molecular magnetism

### Introduction

The design of molecules that can be utilized for information processing and data storage is an attractive goal in present material science. Considerable efforts have been devoted to improve the performance of spin transition materials, in order, to realize their applications as molecular switches, nanosensors, data storage and display devices. However, most spin transition materials reported so far have experienced spin transition at low temperatures rather than room temperature due to the thermal equilibrium between high spin (HS) and low spin (LS) states with a moderate ligand field. However, one of the great challenges underlying the search for such molecule-based functional materials is to produce systems that exhibit properties of technological interest that can be tuned and exploited at room temperature. Thermal hysteresis is crucial to the molecular bistability and information storage, a wide hysteresis near room temperature is

expected to be of practical sense for the molecular compounds. Some landmark achievements in this area are the discovery of a molecule-based magnet that displays ordering above 300K [1,2], and the preparation of molecular materials that undergo spin transitions close to room temperature [3].

In octahedral ligand fields, transition metal ions with  $d^4$ - $d^7$  configurations adopt either a high-spin (HS) or a low spin (LS) electronic arrangement, according to whether the crystal field energy is lower or higher than the mean spin pairing energy. If the two energies are comparable, transitions between the two spin states can be brought about by varying the temperature for example. In many cases, particularly for ferrous compounds, bistability takes place, in other words the LS-HS and HS-LS transitions occur at different temperatures, forming a hysteresis loop. Materials, in which thermally induced spin transitions take place near room temperature, are interesting in view of their possible use as molecular electronic devices intended for the purpose of information recording and processing [4,5].

Such spin transitions are triggered by external perturbations, such as electromagnetic radiation, magnetic fields, and pressure/temperature variations. Within crystalline phases, the response to the spin transition may be transmitted in a cooperative manner throughout the material, leading to hysteretic behaviour [6]. Such molecular solid state systems show characteristics of bistability, and can therefore be considered for an application as molecular switches. Current efforts are aimed at integrating spin transition systems into metal organic frameworks, to combine their properties, such as chirality, conductivity, or those derived from nanoporosity. The molecular approach used to prepare hybrid materials has been mostly exploited to obtain networks that exhibit a wide range of pore size and shapes [7,8] and which have the added potential of offering a variety of other functions, in particular, because of the inclusion of transition metals [9]. This may lead to systems where the multifunctionality is manifested by the coexistence of more than one property, such as ferromagnetism and metal conductivity [10], with no mutual interdependence. The presence of different functions within a material can, however, occur in such a way that they influence each other in a synergetic manner, thereby producing effects that would not be observed, if these properties were not coupled. Remarkable examples are, for instance, the observation of a switchable dielectric constant in a material controlled by the spin state of its spin transition centers [11], or the ability to modify the spin transition properties of a nanoporous framework by changing the nature of its guest molecules [12].

### Temperature-dependent Spin Transition

#### Definition of spin transition

Atoms of first-row transition metals with electronic configurations  $d^4$ - $d^7$  ( $Cr^{II}$ ,  $Mn^{III}$ ,  $Fe^{III}$ ,  $Mn^{II}$ ,  $Fe^{II}$ ,  $Co^{III}$ ,  $Co^{II}$ ) in an octahedral symmetry can adopt two different electronic ground states according to the occupation of the d orbitals split into the  $e_g$  and  $t_{2g}$  subsets. When the energy difference between these orbitals ( $\Delta$ ) is greater than the interelectronic repulsion energy ( $P$ ), the electrons tend to occupy the orbitals of lower energy  $t_{2g}$ , and the configuration of the central

\*Corresponding author: Nayathuparambil Thomas Madhu, Department of Chemistry, Addis Ababa Science and Technology University, Addis Ababa, P.O.Box.16417, Ethiopia, Tel: ++43-1-58801-15350; Fax: ++43-1-5816668-16299; E-mail: ntmadhu@hotmail.com

Wolfgang Linert, Institute of Applied Synthetic Chemistry, Vienna University of Technology, Getreidemarkt 9/163-AC, A-1060 Vienna, Austria, Tel: ++43-1-58801-163613; Fax: ++43-1-58801-9-163613; E-mail: wolfgang.linert@tuwien.ac.at

Received: October 06, 2017 Accepted: October 14, 2017 Published: October 21, 2017

metal ion is low spin (LS). In contrast, when  $\Delta < P$ , the d electrons obey Hund's rule, and the metal complex adopts the high-spin state (HS).

In-between these limits of high and low spin, a situation, where the crystal field energy and interelectronic repulsion energy have similar values, can occur. Here, the difference in energy between the HS and LS states is on the order of the magnitude of the thermal energy  $kT$ . The spin state of this type of molecule depends only on external conditions ( $T, p, B$ ), and this kind of phenomenon is termed "spin transition" (ST) or "spin crossover" (SC) herein (Figure 1).

### Classification of spin transitions

Temperature-dependent spin transitions occur in the crystalline and amorphous solid states, as well as in liquid solutions. In the latter case, the molar fraction of complex molecules in the HS state as a function of the temperature  $X_{HS}(T)$  always follows a simple Boltzmann distribution law for the two states. In the solid state, however, the situation is different. Interactions between the spin-state-changing metal complexes themselves, as well as the complex molecules and the lattice may become very effective, leading to different shapes of  $\chi(T)$  curves, as schematically represented in Figure 2: (a) gradual, (b) abrupt, (c) with hysteresis, (d) plateau, reflecting two (or more) stepped transitions, and (e) a transition with a residual HS fraction at low temperatures. In view of potential solid-state applications, abrupt and complete spin transitions exhibiting a wide hysteresis around room temperature would be of great interest [13,14]. In Figure 2, the state of the art for spin transitions measured against the criteria mentioned above will be reviewed and discussed.

#### Room-temperature spin transition systems

**Iron(II)–triazole complexes:** The majority of room-temperature ST-compounds reported until now are derived from the 1,2,4-triazole (trz) ligand system. Structurally, these complexes consist of linear chains, in which Fe(II) ions are linked by triple  $N1,N2$ -1,2,4-triazole bridges (Figure 3).

A series of iron(II) coordination polymers of 4-octadecyl-1,2,4-triazole have been synthesized and their spin transition properties have been investigated in detail [15,16]. Thus, the introduction of the tosylate counter anion led to a sharp spin transition close to room

temperature ( $T_{1/2} \sim 300$  K) with a rather large hysteresis of ca.  $\Delta T_{1/2} = 15$  K. It is interesting to note that water has been found to be a good solvent for the synthesis of iron(II)–triazole coordination polymers. Generally, these complexes are highly cooperative and counter anion exchange has been proven to be a versatile way to fine-tune the spin transition temperature.

Kahn et al. [17] reported the spin transition properties of the compound  $\{[\text{Fe}^{\text{II}}(\text{Htrz})_2(\text{trz})]\}_n(\text{BF}_4)_n$  and  $\{[\text{Fe}^{\text{II}}(\text{Htrz})_3]\}_n(\text{BF}_4)_{2n} \cdot (\text{H}_2\text{O})_n$ , (where Htrz and trz are the protonated and deprotonated forms of 1,2,4-triazole). The ST of the first compound,  $\{[\text{Fe}^{\text{II}}(\text{Htrz})_2(\text{trz})]\}_n(\text{BF}_4)_n$ , is strongly dependent on the parameters of the synthesis. In a water/ethanol mixture, a polymorph  $\{[\text{Fe}^{\text{II}}(\text{Htrz})_2(\text{trz})]\}_n(\text{BF}_4)_n$  (A) is formed, which exhibits a very abrupt spin transition, centered around 360 K, with a thermal hysteresis of 50 K, while the polymorph  $\{[\text{Fe}^{\text{II}}(\text{Htrz})_2(\text{trz})]\}_n(\text{BF}_4)_n$  (B) prepared in pure methanol leads to a smoother transition with a reduced hysteresis width. The spin transition parameters of polymorph (A) depend also strongly on the number of temperature cycles: In the first cycle, polymorph A shows STs at  $T_{1/2\uparrow} = 345$  K and  $T_{1/2\downarrow} = 385$  K (up and down), while  $T_{1/2\uparrow}$  is progressively shifted towards higher temperatures during the following four cycles, finally reaching a hysteresis loop of 50 K. This behavior is explained by some kind of "running in" of the material. The magnetic behavior of polymorph (B) exhibits a less abrupt ST with a hysteresis loop width of about 50 K. Again, successive thermal cycles modify the ST parameters of this compound. The width of the thermal hysteresis loop is reduced by more than 50% after three cycles (Figure 4).

In fact, compound  $\{[\text{Fe}^{\text{II}}(\text{Htrz})_3]\}_n(\text{BF}_4)_{2n} \cdot (\text{H}_2\text{O})_n$  was found to undergo an  $\alpha \leftrightarrow \beta$  phase transition around 420 K, whereby the two phases exhibit different ST behaviors. The  $\alpha$  phase shows a rather abrupt spin transition centered around 335 K with a thermal hysteresis of  $\Delta T_{1/2} = 22$  K. The  $\beta$  phase is metastable at room temperature and shows an abrupt ST around room temperature with a hysteresis of  $\Delta T_{1/2} = 6$  K (Figure 5). The water-free compound  $\{[\text{Fe}^{\text{II}}(\text{Htrz})_3]\}_n(\text{BF}_4)_{2n}$  exhibits a less abrupt ST with a smaller hysteresis compared to its hydrated equivalent.

Nanoparticles of  $\{[\text{Fe}^{\text{II}}(\text{Htrz})_2(\text{trz})]\}_n(\text{BF}_4)_n$  have been prepared by the reverse micelle technique [18]. Transmission electron microscopy

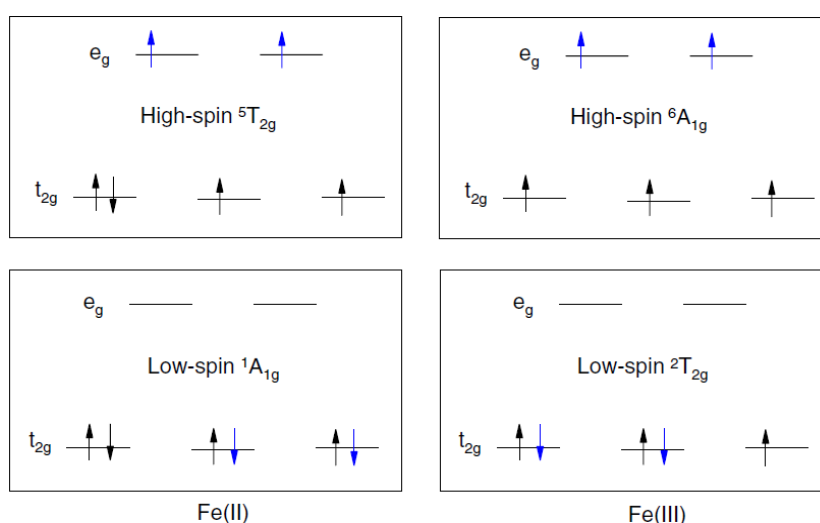


Figure 1: d-orbitals of Fe-complexes (both Fe<sup>II</sup> and Fe<sup>III</sup>) showing transitions between low-spin and high-spin in an octahedral ligand field.

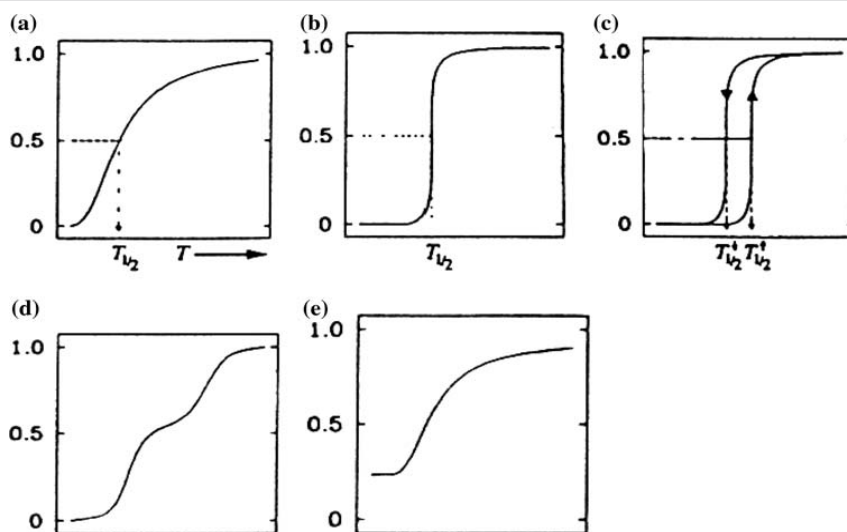


Figure 2: Various types of spin state transition curves: (a) gradual, (b) abrupt, (c) with hysteresis, (d) two-step transition and (e) incomplete.

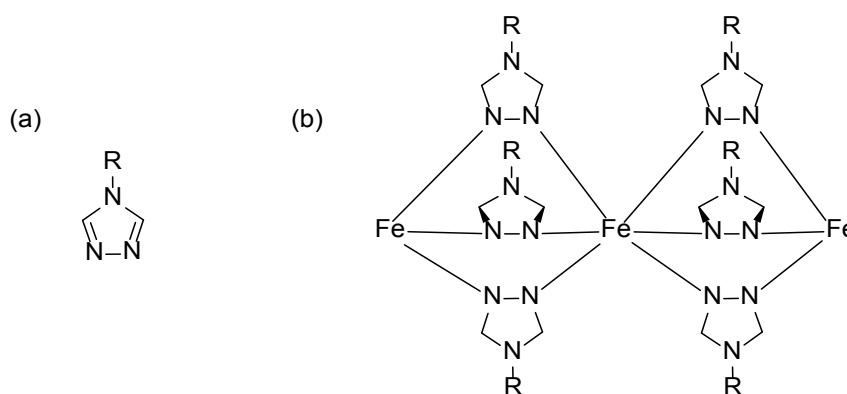


Figure 3: Structures of the trz ligand-system (a) and the corresponding coordination polymerchain  $\{[Fe^{II}(trz)_3]^{2+}\}_n$  (b) with trz = 1,2,4 triazole and R representing different substituents.

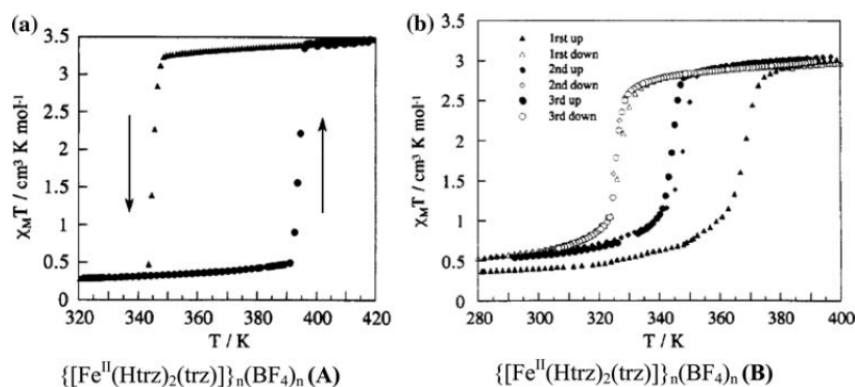


Figure 4: Magnetic properties ( $\chi_M T$  vs  $T$ ) of two polymorphs of the coordination polymer  $\{[Fe^{II}(Htrz)_2(trz)]\}_n(BF_4)_n$ . (A) prepared in an ethanol/water mixture (B) prepared in methanol.

(TEM) images show that the average nanoparticle size is below 20 nm. The clear deep purple suspensions of these nanoparticles in n-octane are stable for a short period of time. In addition, the solid produced by controlled evaporation of the solvent can be resuspended to yield

a bright transparent suspension. This suspension does indeed turn light pink when heated up, maintaining this color until it cools down below 70°C. Both colors, each associated with the high- and low-spin states, respectively, are stable for a wide range of temperatures.

The suspension of  $\{[\text{Fe}^{\text{II}}(\text{Htrz})_2(\text{trz})]\}_n(\text{BF}_4)_n$  nanoparticles was dried by removing the solvent in vacuum. Magnetic measurements were performed on the solid residue show that the spin transition of the nanoparticles is clearly preserved in the solid state, and it remains almost identical to that reported for bulk samples. The transition is very abrupt, rendering a well-shaped thermal hysteresis loop over 40 K (Figure 6).

It can also be observed that slight modifications of the synthetic procedure (eg. different ratios of the used solvents, water, and surfactants) lead to different micelle sizes, which affect the sizes of the particles and their ST properties. The critical temperatures can be lowered towards room temperature by changing the composition of the nanoparticles by doping the  $\{[\text{Fe}^{\text{II}}(\text{Htrz})_2(\text{trz})]\}_n(\text{BF}_4)_n$  nanoparticles with 20% Zn(II) metal ions.

The syntheses and spin transition properties of the compounds  $\{[\text{Fe}(\text{Htrz})_3]\}_2(\text{ClO}_4)_{2n}$  and  $\{[\text{Fe}(\text{Htrz})_{3-3x}(4\text{-NH}_2\text{trz})_{3x}]\}_n(\text{ClO}_4)_{2n} \cdot n\text{H}_2\text{O}$  (Htrz = 1,2,4-tiazole, 4-NH<sub>2</sub>trz = 4-amino-1,2,4-triazole) have been reported [19]. The perfectly dry perchlorate analogue,  $\{[\text{Fe}(\text{Htrz})_3]\}_n(\text{ClO}_4)_{2n}$ , shows a rather smooth ST around 265 K with a weak hysteresis of about 5 K. When a drop of water is added to 50 mg of  $\{[\text{Fe}(\text{Htrz})]\}_n(\text{ClO}_4)_{2n}$ , the transition becomes very abrupt in the warming and cooling modes, with  $T_{1/2}(\uparrow) = 313$  K and  $T_{1/2}(\downarrow) = 296$  K. The water molecules create hydrogen bonds, which increases the cooperation between the Fe<sup>II</sup>-centers. The ST is accompanied by an intense color change from purple to white. The hysteresis loop is just above room temperature and can be shifted by ligand doping with the 4-NH<sub>2</sub> trz ligand. Since the compound  $\{[\text{Fe}(4\text{-NH}_2\text{trz})]\}_2(\text{ClO}_4)_{2n}$  shows a smooth transition, centered around 130 K, the authors expect that the ST properties could be controlled by the addition of the ligands 4-NH<sub>2</sub>trz and Htrz. Consequently, the magnetic properties of the material  $\{[\text{Fe}(\text{Htrz})_{3-3x}(4\text{-NH}_2\text{trz})_{3x}]\}_n(\text{ClO}_4)_{2n} \cdot n\text{H}_2\text{O}$  were investigated for compositions  $0 \leq x \leq 0.1$ , and the authors found the dependences  $T_{1/2}(\uparrow) = 313 - 180x$  and  $T_{1/2}(\downarrow) = 296 - 160x$ . With  $x = 0.05$ , the transition occurs with hysteretic branches above and below room temperature, with  $T_{1/2}(\uparrow) = 288$  K and  $T_{1/2}(\downarrow) = 304$  K (Figure 7).

Kahn et al. [20] reported the spin transition properties of the compound  $\{[\text{Fe}^{\text{II}}(4\text{-NH}_2\text{trz})_3]\}_n(\text{tos})_{3n} \cdot 2\text{H}_2\text{O}$ , (tos = tosylate anion) under hydrated and dehydrated conditions. The hydrated form exhibits an abrupt spin transition in the warming regime at 361 K accompanied by the removal of the two noncoordinated water molecules. Cooling the dehydrated compound,  $\{[\text{Fe}(\text{NH}_2\text{trz})_3]\}_n(\text{tos})_{3n}$ , causes a slightly smoother spin transition at 279 K. In the presence of humidity and at room temperature (293 K), the white  $\{[\text{Fe}^{\text{II}}(4\text{-NH}_2\text{trz})_3]\}_n(\text{tos})_{3n}$  turns back into the violet hydrated phase. The dehydration allows the isolation of a system with an exceptionally large thermal hysteresis loop of ca. 80 K. The  $\{[\text{Fe}^{\text{II}}(\text{NH}_2\text{trz})_3]\}_n(\text{tos})_{3n} \cdot 2\text{H}_2\text{O} - \{[\text{Fe}^{\text{II}}(\text{NH}_2\text{trz})_3]\}_n(\text{tos})_{3n}$  couple was one of the first examples of spin transition materials with a large hysteresis that exhibited up and down branches below and above room temperature.

The polymeric compound  $\{[\text{Fe}^{\text{II}}(4\text{-NH}_2\text{trz})_3]\}_n(\text{NO}_3)_{2n}$  (with NH<sub>2</sub>trz = 4-amino-1,2,4-triazole) was characterized and studied by optical response and electron spin resonance using Cu<sup>2+</sup> and Mn<sup>2+</sup> as dopants and paramagnetic probes [21]. In all of the doped samples the spin transition of Fe<sup>2+</sup> ions was characterized by a pronounced thermochromic effect between a bright pink color (LS state) and chalky white colors (HS state), so the ST could be detected in an optical manner. It could be observed that doping with copper does not affect  $T_{1/2}(\uparrow)$ , while the stabilized  $T_{1/2}(\uparrow)$  value is more sensitive to doping. By changing the amount of dopant from 10 % to 1 %, the hysteresis loop for the Cu/Fe-doped sample shifts its center from 312 to 307 K.

Simultaneously, the hysteresis loop narrows from 36 K down to 28 K and the ST becomes less abrupt. Doping the same compound with manganese(II) has a more pronounced effect upon the characteristics of the hysteresis loop, which dramatically narrows over the course of the first three thermal cycles (from 41 K to a stabilized value of 21 K). Finally, the hysteresis loop  $\Delta T_{1/2}$  narrows and  $T_{1/2}$  shifts to a lower temperature with increasing manganese(II) doping level.

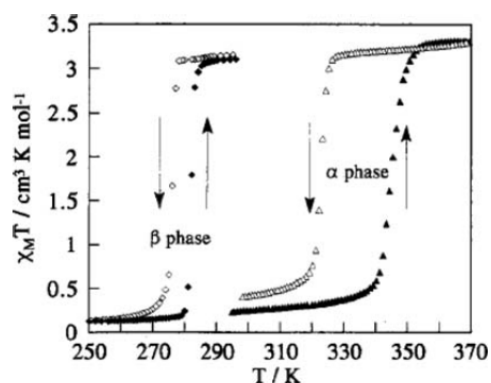


Figure 5: Magnetic properties of the two different crystalline phases (α and β) of the coordination polymer  $\{[\text{Fe}(\text{II})(\text{Htrz})_3]\}_n(\text{BF}_4)_{2n} \cdot (\text{H}_2\text{O})_n$ .

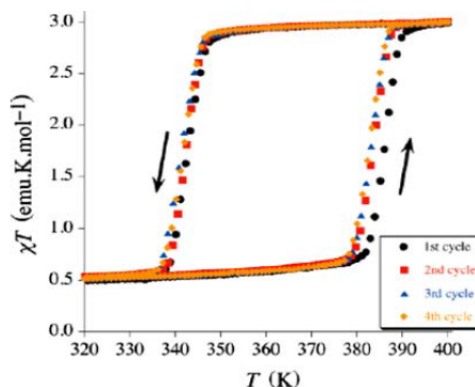


Figure 6:  $\chi_M T$  versus  $T$  plot for four cooling/heating cycles of  $\{[\text{Fe}(\text{II})(\text{Htrz})_2(\text{trz})]\}_n(\text{BF}_4)_n$  nanoparticles (20nm) showing the thermal hysteresis.

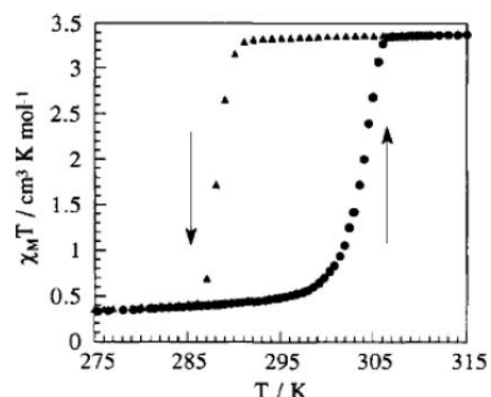


Figure 7:  $\chi_M T$  versus  $T$  plot for  $\{[\text{Fe}(\text{Htrz})_{3-3x}(4\text{-NH}_2\text{trz})_{3x}]\}_n(\text{ClO}_4)_{2n} \cdot n\text{H}_2\text{O}$  with  $x = 0.05$ , exhibiting a spin transition with a wide hysteresis around room temperature.

Further anion exchange generated a series of iron(II) spin transition compounds of the general formula  $\{[\text{Fe}^{\text{II}}(4\text{-NH}_2\text{trz})_3]\}_n \text{X}_{2n} \cdot x\text{H}_2\text{O}$  ( $\text{X} = 1\text{-naphthalene sulfonate, 2-naphthalene sulfonate, 4-hydroxy-1-naphthalene sulfonate, 4-amino-1-naphthalene sulfonate, 6-hydroxy-2-naphthalene sulfonate}$ ), and the ST properties of these were investigated in relation to the nature of the counter anion involved [22]. These compounds are isostructurally linear chains, in which iron(II) ions are linked by  $\text{N}^1, \text{N}^2$  of 1,2,4-triazole bridges, while the non-coordinating anions of naphthalene sulfonate type mediate interchain interactions. The physical properties of these compounds can be understood by the synergy between the Fe(II) spin transition behavior and by the dehydration-hydration process for interstitial water solvent molecules. In terms of room-temperature ST, the compound involving the 2-naphthalene sulfonate anion delivers a temperature-induced hysteresis centered at 290 K and with a 14 K hysteresis width. A further series of iron(II) ST compounds of the general formula  $\{[\text{Fe}^{\text{II}}(\text{hyetrz})_3]\}_n (\text{X})_{2n} \cdot x\text{H}_2\text{O}$ , where  $\text{hyetrz} = 4\text{-}(2'\text{-hydroxyl-ethyl})\text{-1,2,4-triazole}$  and  $\text{X} = \text{Cl}^-, \text{NO}_3^-, \text{Br}^-, \text{I}^-, \text{BF}_4^-, \text{ClO}_4^-$  and  $\text{PF}_6^-$ , have been prepared [23]. Here, the ST is strongly associated with the removal of lattice water molecules, which initially stabilize the low-spin state. However, after dehydration, the perchlorate and iodide variants show clearly increased transition temperatures. In general, a correlation, where the transition temperature  $T_{1/2}$  increases with increasing anion radius was found. For example, in  $\{[\text{Fe}^{\text{II}}(\text{hyetrz})_3]\}_n (\text{I})_{2n}$ , the ST temperature  $T_{1/2}$  gets very close to room temperature, and is accompanied by a thermal hysteresis of 12K centered in the vicinity of room temperature (291K). Thus,  $\{[\text{Fe}^{\text{II}}(\text{hyetrz})_3]\}_n (\text{I})_{2n}$  represents one of the very few iron(II) spin transition materials, which show a spin transition with hysteresis and to be associated with thermochromic effects in the close vicinity of room temperature.

The synthesis, structural characterisation, Mössbauer study and magnetic properties of a trinuclear iron(II) compound containing the hyetrz ligand,  $[\text{Fe}_3^{\text{II}}(\text{hyetrz})_3(\text{H}_2\text{O})_6](\text{CF}_3\text{SO}_3)_3$ , were reported by Güttlich et al. [24]. Single-crystal X-ray structure analysis carried out at two different temperatures (120 and 330 K) reveal that the central iron Fe1 is coordinated to six 4-(2'-hydroxyl-ethyl)-1,2,4-triazole nitrogens, while the two peripheral equivalent irons, Fe2 and Fe2', are coordination polyhedral, contain three hyetrz nitrogens and three water oxygens (Figure 8).

Hydrogen bonding via the  $\text{SO}_3$  oxygen atoms of the triflate anions link to the coordinated water molecules, and these anions are also linked by hydrogen bonding to the hydroxyl groups of the ethyl chain in the 4-position of each triazole ligand. The bond distances of the central iron Fe1 change with the temperature, indicating a LS state at

120 K and a HS state at 330 K. However, the bond lengths of the Fe2 and Fe2' polyhedra remain constant with the temperature and thus are iron(II) in the HS state.

Magnetic measurements (Figures 8 and 9) reveal a gradual ST behavior, which crosses the room temperature regime. In the temperature range between 77–235 K, the  $\chi^T$  value is constant and equal to 7.4  $\text{emu K mol}^{-1}$ , which corresponds to two HS iron(II) centers and confirms the predictions of the X-ray structure at low temperature. Above 240 K the magnetic moment increases with the temperature, and at 360 K it reaches the value 10.92  $\text{emu K mol}^{-1}$ , which is in accordance with the situation, where the molecule contains three iron(II) HS centers.

The synthesis, characterization, spin cross over characteristics and Mössbauer characterization of Fe(II) complexes of the tripoidal ligand tris[(1-benzyl-1H-1,2,3-triazol-4-yl)methyl]amine (tba) (Figure 9), have been reported by Sarkar et al. [25].

The Fe center in complex  $[\text{Fe}(\text{tba})_2](\text{BF}_4)_2$  (Figure 10) is bound to two triazole and one amine N atom from each tba ligand, with the third triazole arm remaining uncoordinated. The benzyl substituents of the uncoordinated triazole arms and the triazole rings engage in strong intermolecular and intramolecular noncovalent interactions. The Fe(II) center in the complex is octahedrally coordinated by two triazole and one amine N donor from each tba ligand. The Fe–N11 and Fe–N21 distances (Fe–N(triazole)) are 1.948(1) and 1.960(2) Å, respectively. The Fe–N1 (Fe–N(amine)) distance is 2.150(1) Å. The Fe–N distances here are typical for a LS  $\text{Fe}^{\text{II}}$  center.

The solvent free compound  $[\text{Fe}(\text{tba})_2](\text{BF}_4)_2$  shows a spin transition near room temperature as shown by magnetic measurement at variable temperature (Figure 11) and spectral Mössbauer characterization.

Brooker et al. reported [26] spin transition properties of the Fe(II) thioether-linked PSRT (4-substituted-3,5-bis[(2-pyridylmethyl)sulfanyl]methyl]-4H-1,2,4-triazoles) ligands (Figure 12).

Single crystal structures of the complexes revealed that these are the first examples of binuclear  $\text{Fe}^{\text{II}}$  complexes with a  $\text{N}_4\text{S}_2$  coordination. In the PSpHT complex, the two equivalent iron(II) atoms are in a distorted octahedral  $\text{N}_4\text{S}_2$  coordination sphere with the two ligands supplying all 12 donor atoms and providing two triazole bridges between each other. Each bridging triazole ligand binds the two iron(II) centers in a trans-axial mode, i.e., with one pyridine arm up and one down relative to the triazole ring. The Fe–N bonds [2.116(16)–2.1569(17) Å] and Fe–S bonds [2.5379(6) and 2.5932(6) Å] are long, the cis angles of the iron(II) coordination sphere ranges around 90° [79.56(5)–

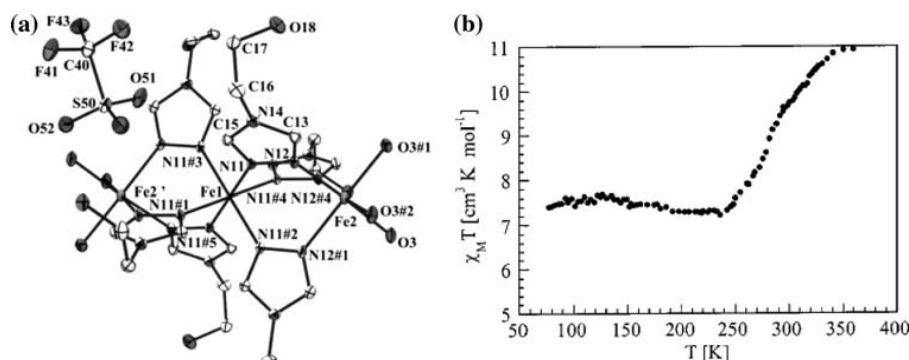


Figure 8: Crystal structure (a) and magnetic properties (b) of compound  $[\text{Fe}_3^{\text{II}}(\text{hyetrz})_3(\text{H}_2\text{O})_6](\text{CF}_3\text{SO}_3)_3$ .

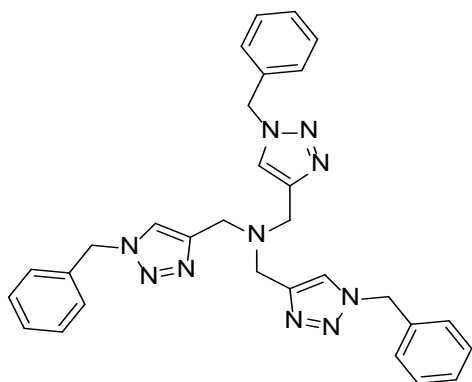


Figure 9: Ligand tris[(1-benzyl-1H-1,2,3-triazol-4-yl)methyl]amine (tbta).

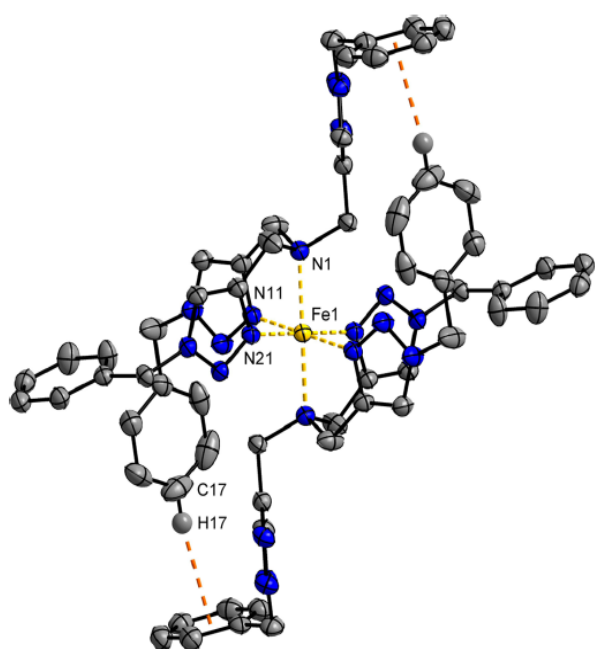


Figure 10: Crystal Structure of [Fe(tbta)2](BF4)2. Crystal Structure of [Fe(tbta)2](BF4)2.

108.06(7)°, and the octahedral distortion parameter is large ( $\Sigma = 109.84^\circ$ ), all of which is consistent with the presence of HS iron(II) centers at 100 K. The PSMePhT complex is isomorphous with the PSPHT complex, so again the iron(II) centers are in an  $N_4S_2$  distorted octahedral environment, and the bridging triazole ligands bind in the trans-axial mode. The Fe-N bonds [2.0885(30)–2.1171(35) Å] and Fe-S bonds [2.4996(12) and 2.5159(14) Å] are shorter than those in [Fe<sup>II</sup><sub>2</sub>(PSPHT)<sub>2</sub>](BF<sub>4</sub>)<sub>4</sub>·2MeCN·H<sub>2</sub>O, but are still within the range, expected for HS iron(II). In the PSiBuT complex, similar to the other two structures, the Fe<sup>II</sup> centers are in a distorted octahedral  $N_4S_2$  coordination sphere, comprising two heterocyclic nitrogen donors and one thioether sulfur donor from each of the two PSiBuT ligands. The length of the Fe-N bonds [2.1273(45)–2.1683(45) Å] and the Fe-S bonds [2.5448(14) and 2.5822(21) Å] are all consistent with the complex being in the [HS-HS] state at 100 K.

All three complexes undergo spin transitions at or near room temperature (Figure 13). It is interesting to mention that the spin

transition properties vary by the exchange of the R-group in the ligand's structure.

**Hoffman-type pyrazine networks:** Real et al. [27] reported about bimetallic coordination complexes of the general formula {[Fe<sup>II</sup>(pz)M<sup>II</sup>(CN)<sub>4</sub>]}<sub>n</sub>·xH<sub>2</sub>O (pz = pyrazine, CN = cyano, M = Ni, Pd, Pt). The crystal structure of this analogue can be seen in (Figure 14a).

The crystal structure displays that two-dimensional sheets of iron-tetracyanoplatinum moieties, which are connected via Fe<sup>II</sup>-pyrazine

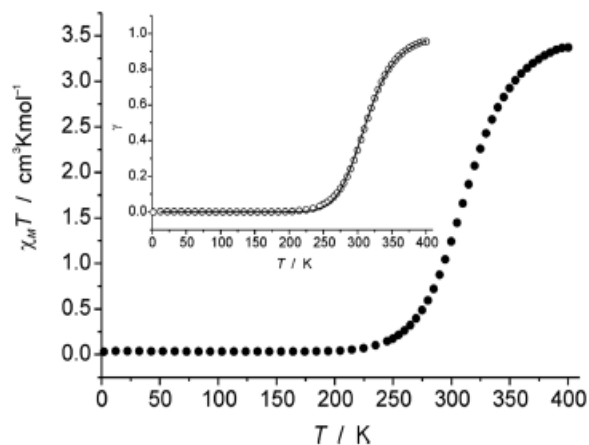


Figure 11: Variable-temperature magnetic susceptibility data of [Fe(tbta)2](BF<sub>4</sub>)<sub>2</sub>.

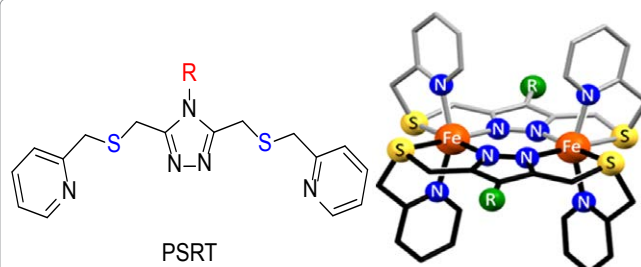


Figure 12: Structure of the ligands PSRT and their Dimeric Fe<sup>II</sup> complexes (Where R = Ph, iBu, and MePh).

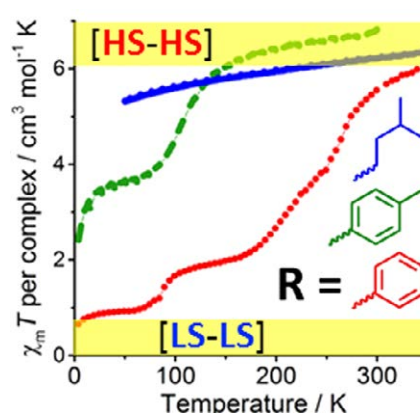


Figure 13:  $\chi_m T$  vs temperature of air-dried crystals of [Fe<sup>II</sup>(PSPHT)<sub>2</sub>](BF<sub>4</sub>)<sub>4</sub>·2.5H<sub>2</sub>O (solvatomorph C), [Fe<sup>II</sup>(PSMeHT)<sub>2</sub>](BF<sub>4</sub>)<sub>4</sub>·1.5MeCN·2H<sub>2</sub>O and [Fe<sup>II</sup>(PSiBuT)<sub>2</sub>](BF<sub>4</sub>)<sub>4</sub>·MeCN·H<sub>2</sub>O.

linkers to a 3D network, were formed. Magnetic measurements of this compound reveal a ST ( $T_{1/2}(\uparrow) = 220$  K and  $T_{1/2}(\downarrow) = 240$  K) with strong hysteretic behavior ( $\Delta T_{1/2} = 20$  K). In another communication, Bousseksou et al. [28] describes the dependence of the ST of the same compound on the presence of interstitial water molecules. Note that the dehydrated form exhibits improved spin transition behavior, exhibiting a more complete ST that is closer to room-temperature. Moreover, the hysteresis loop becomes wider ( $\Delta T_{1/2} = 24$  K), rather square-shaped, and reproducible over several cycles (Figure 14b).

Additionally, and for the first time, a reversible light induced LS  $\leftrightarrow$  HS one-shot laser excitation within the area of the hysteresis loop was observed. This is of fundamental importance, because in contrast to light-induced spin state trapping (LIESST), this experiment even works at room temperature, and does not show thermal relaxation from HS to LS. The metastable HS- or LS-states have infinite lifetimes in the thermal hysteresis loop region, which may give access to switch a behavior, which could be exploited in molecular hybrid device setups [28].

A ST around room temperature with a hysteresis can also be observed for the nickel analogue of the 3D Hoffman-type pyrazine network,  $\{[\text{Fe}^{\text{II}}(\text{pz})][\text{Ni}^{\text{II}}(\text{CN})_4]_n \cdot 2\text{H}_2\text{O}\}$ , but the transition is not that

abrupt and the hysteresis is smaller ( $T_{1/2}(\uparrow) = 280$  K and  $T_{1/2}(\downarrow) = 305$  K) than for the compound described before [27].

With respect to the aim to use spin transition compounds in the field of memory storage devices, Hoffman-type pyrazine networks are excellent candidates due to their unique combination of abrupt spin transitions with wide thermal hysteresis loops, which are centered around room temperature. Furthermore, Cobo et al. [29] studied the surface-assisted creation of multilayers of this class of ST compounds. The first monolayer cycle was obtained from a mercaptopyridine surface link (Figure 15a, step 1), while the conventional pyrazine ligand was used during subsequent cycles.

Alternating coordination sequences of iron(II) ions,  $[\text{Pt}^{\text{II}}(\text{CN})_4]^{2-}$  and pyrazine finally led to an architecture of a few multilayers of water-free  $\{[\text{Fe}^{\text{II}}(\text{pz})\text{Pt}^{\text{II}}(\text{CN})_4]_n\}$  on a gold substrate (Figure 15a, step 2-4). The ST properties of the assembled thin films were subsequently studied by variable-temperature Raman spectroscopy. The Raman spectra of both, a powder sample and the multilayer were measured at several temperatures in the cooling and heating mode. The powder sample reveals a hysteresis loop width of 25 K centered around 290 K, corresponding closely to the magnetic susceptibility measurements (Figure 16a).

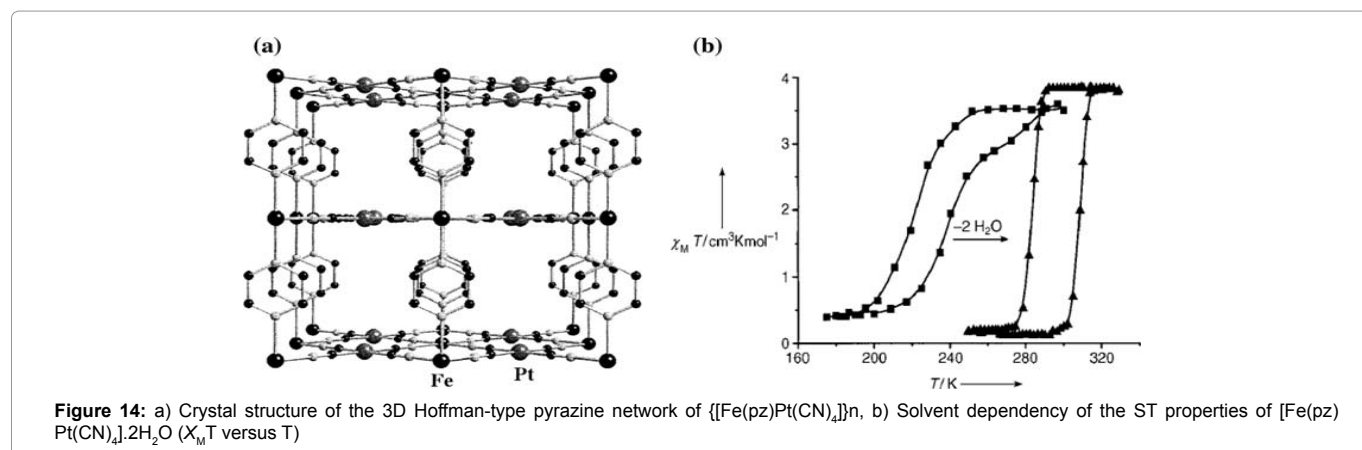


Figure 14: a) Crystal structure of the 3D Hoffman-type pyrazine network of  $\{[\text{Fe}(\text{pz})\text{Pt}(\text{CN})_4]_n\}$ , b) Solvent dependency of the ST properties of  $[\text{Fe}(\text{pz})\text{Pt}(\text{CN})_4] \cdot 2\text{H}_2\text{O}$  ( $\chi_M T$  versus  $T$ )

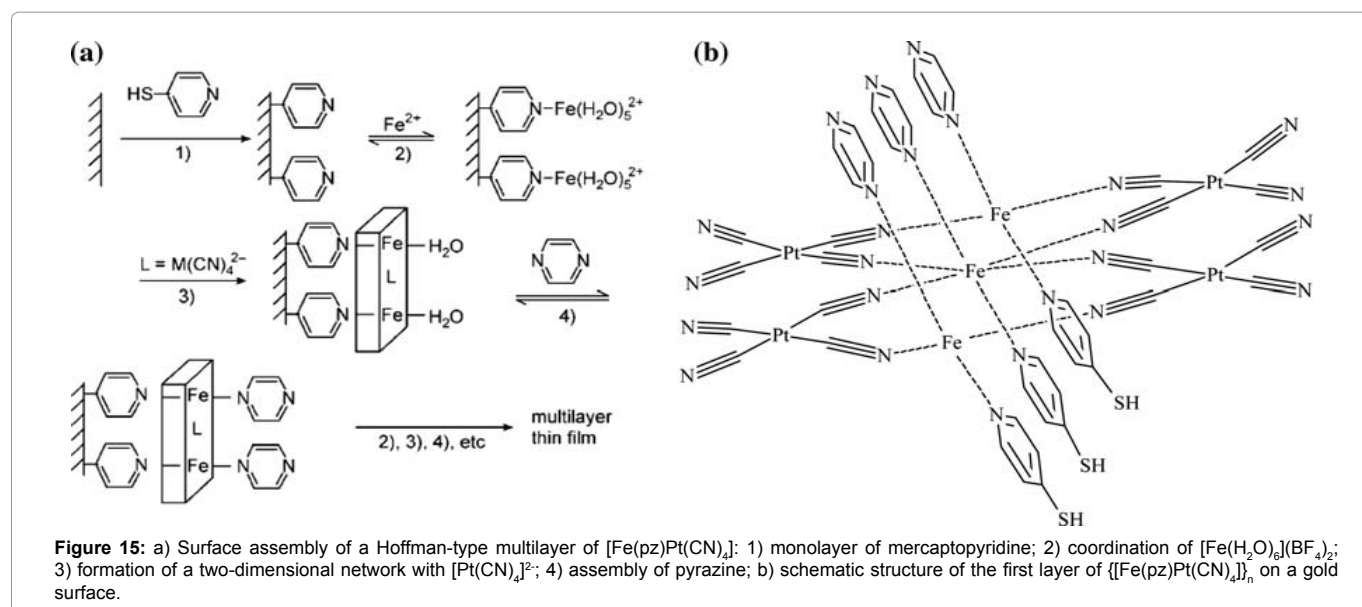


Figure 15: a) Surface assembly of a Hoffman-type multilayer of  $[\text{Fe}(\text{pz})\text{Pt}(\text{CN})_4]$ : 1) monolayer of mercaptopyridine; 2) coordination of  $[\text{Fe}(\text{H}_2\text{O})_6](\text{BF}_4)_2$ ; 3) formation of a two-dimensional network with  $[\text{Pt}(\text{CN})_4]^{2-}$ ; 4) assembly of pyrazine; b) schematic structure of the first layer of  $\{[\text{Fe}(\text{pz})\text{Pt}(\text{CN})_4]_n\}$  on a gold surface.

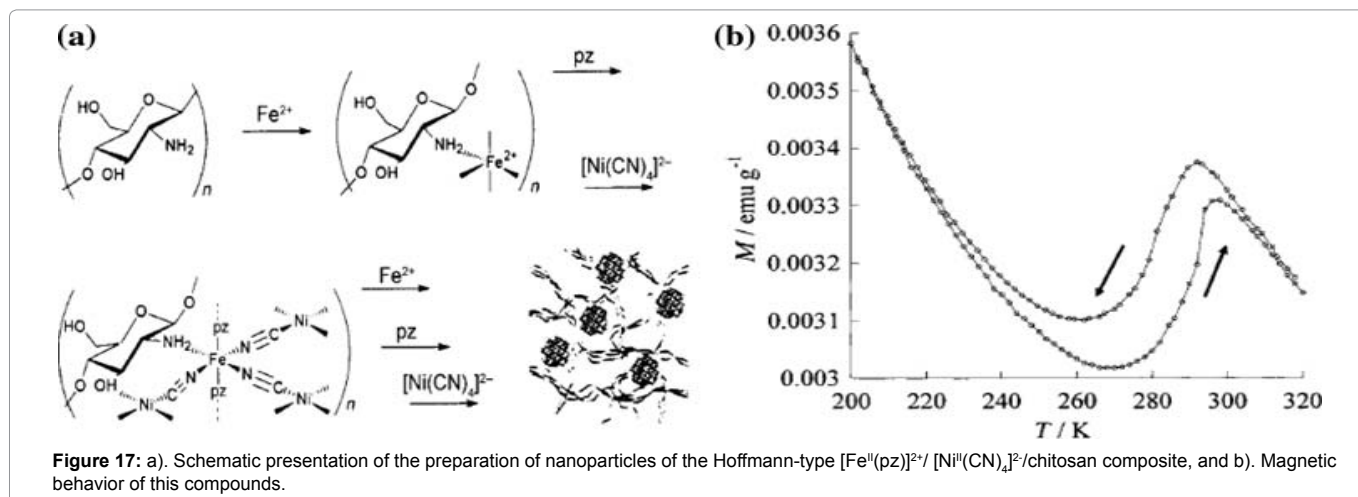
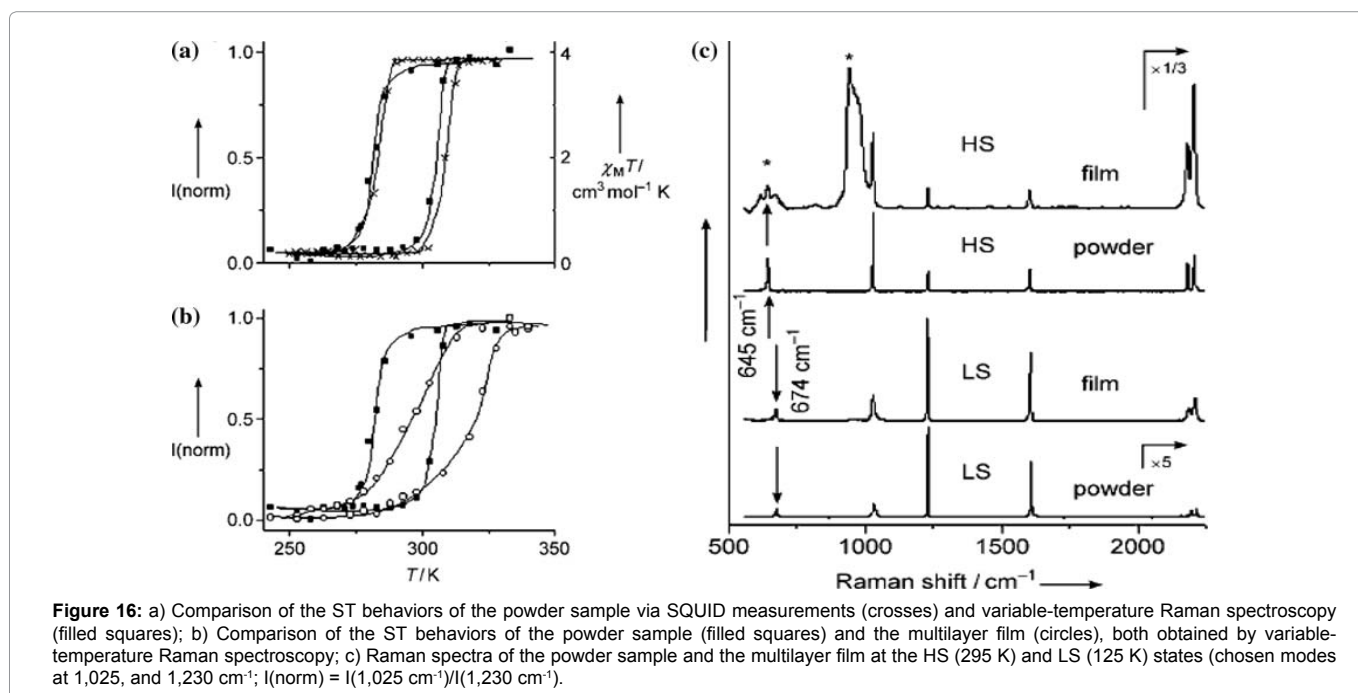
The multilayer sample displays a hysteresis loop centered around 310 K, also showing a hysteresis width of 25 K. However, the ST in the multilayers is much less abrupt and the square shape of the hysteresis loop has completely vanished (Figure 16b). The authors normalized the Raman intensity by the formula  $I(\text{norm}) = I(1,025 \text{ cm}^{-1}) / I(1,230 \text{ cm}^{-1})$ , since the modes at 1,025  $\text{cm}^{-1}$  and 1,230  $\text{cm}^{-1}$  have the highest intensity, but other Raman markers provided comparable results (Figure 16c).

The ST behavior of nanoparticles made of Hoffman type pyrazine networks was reported by Larionova et al. [30]. The authors studied  $[\text{Fe}^{\text{II}}(\text{pz})]^{2+}$ - and  $[\text{Ni}^{\text{II}}(\text{CN})_4]^{2-}$ -chitosan composite beads (Figure 17).

The determination of the magnetic properties of the material was obtained at fields of 1T. The results reveal incomplete STs ( $T_{1/2}(\uparrow) = 220 \text{ K}$  and  $T_{1/2}(\downarrow) = 240 \text{ K}$ ) for this kind of nanoparticles and a 10 K thermal hysteresis width. Variable-temperature Mössbauer investigations confirm the loss of ST in the nanoparticle material.

Obviously, only one third iron(II) ions undergo a ST, while two-thirds remain in the LS state at any temperature. The huge thermally inactive fraction can be related to the huge surface area to volume ratio of these small nanoparticles (3–5 nm), since 60–70% of the iron atoms are localized at the surface. Thus, most of the iron(II) centers in the nanoparticles experience a strongly modified coordination environment; and this situation leads to ST loss due to an inappropriate ligand field strengths.

In addition to the above mentioned 3D structures, two isostructural compounds expressing 2D coordination polymer networks of the formula  $\{[\text{Fe}^{\text{II}}(3\text{-Xpy})_2\text{AgI}(\text{CN})_2] [\text{Ag}^{\text{I}}(3\text{-Xpy})(\text{CN})_2]\}_n \cdot 3\text{-Xpy}$  (py = pyridine; X = Br, I) were reported [31]. These compounds create 2D corrugated layers. The ST is situated in both cases close to room temperature (eg. for X = I exhibiting a thermal hysteresis,  $T_{1/2}(\uparrow) = 261\text{K}$  and  $T_{1/2}(\downarrow) = 275 \text{ K}$ ). In the bromo analogue, the ST is observed only in the heating mode ( $T_{1/2} = 306 \text{ K}$ ); the compound remains blocked in the HS state during the cooling mode.



**Iron(II) bis(pyrazol)pyridine complexes:** Halcrow et al. [32-35] reported about an iron(II) complex, which contains the tridentate N donor ligand 2,6-bis(pyrazol-1-yl)pyridine (1-bpp) with the formula  $[\text{Fe}(\text{1-bpp})_2](\text{BF}_4)_2$  (Figure 18).

This compound shows an unusually abrupt spin transition centered below room temperature ( $T_{1/2} = 259 \text{ K}$ ) and possessing a mere 3 K thermal hysteresis. This ST is accompanied by significant thermochromism, with dark brown and mustard yellow colors, indicating the LS- and the HS-state, respectively. A substitution in the 4-position of the pyridine ring of the bpp ligand has been found to be a useful tool to increase the ST temperature until they get close to room temperature (Figure 19) [13,36-38].

The introduction of a para-pyridyl substituent leads to the linear interconnection of the mononuclear iron(II) complexes into a chain like hydrogen-bonding polymer  $\{[\text{Fe}^{\text{II}}(\text{1-bpp-4-py-H}^+)(\text{bpp-4-py})]\}_n(\text{ClO}_4)_{3n}(\text{CH}_3\text{OH})_n$  (Figure 20a,c) [36] (1-bpp-4-py = 2,6-bis(pyrazol-1-yl)-4,4'-bipyridine (Figure 19a).

The interconnecting hydrogen bonds are performed by the semi-protonation of the para-pyridine nitrogens of the ligand 1-bpp-4-py, forming pyridinium cations that allow self-complementary N<sup>+</sup>-H-N hydrogen bonds together with deprotonated pyridines of neighbouring complex units, resulting in infinite one-dimensional chains of mononuclear ST Fe<sup>II</sup> centers. The ST of this 1D polymer, which is centered exactly at room temperature, is accompanied by a 2 K hysteresis ( $T_{1/2}(\downarrow) = 285 \text{ K}$ ;  $T_{1/2}(\uparrow) = 287 \text{ K}$ ) and demonstrates the existence of a significant degree of cooperation mediated by hydrogen bonds and/or by the methanol molecules trapped in the lattice. The zero-field <sup>57</sup>Fe Mössbauer spectra of the powdered sample was obtained at several temperatures. No notable difference between the cooling and heating mode was observed and the room-temperature ST of the sample was also confirmed by the data of the Mössbauer spectra.

With a similar system, a ST iron(II) complex, including the ligand 1-bpp-4-acety-ph-SAc (S-(4-[[2,6-(bispyrazol-1-yl)pyrid-4-yl]ethynyl]-phenyl)ethanethioate (Figure 19b), has also been reported [37]. The ST of the resulting complex  $[\text{Fe}^{\text{II}}(\text{1-bpp-4-acety-ph-SAc})_2](\text{ClO}_4)_2$  is situated very close to room temperature ( $T_{1/2}(\uparrow) = 273 \text{ K}$ ;  $T_{1/2}(\downarrow) = 281 \text{ K}$ ). The appearance of its thermal hysteresis ( $\Delta T_{1/2} = 8 \text{ K}$ ) is attributed to intermolecular hydrogen bonding interactions and sulfur-sulfur contact for acetyl protected thiol end-groups. Further substitutions explain the influence of the nature of the 4-substituents on the ST temperature. The iodo analogue,  $[\text{Fe}^{\text{II}}(\text{1-bpp-4-I})_2](\text{ClO}_4)_2$

(1-bpp-4-I = 4-iodo-2,6-bis(pyrazol-1-yl)pyridine (Figure 19c), shows an abrupt ST ( $T_{1/2} = 333 \text{ K}$ ), while the 4-hydroxy phenyl group causes the ST in  $[\text{Fe}^{\text{II}}(\text{1-bpp-4-ph-OH})_2](\text{ClO}_4)_2$  (1-bpp-4-ph-OH = 4-(4-hydroxyphenyl)-2,6-bis(pyrazol-1-yl)pyridine (Figure 19d) to be exactly at room temperature ( $T_{1/2} = 281 \text{ K}$ ), but without a hysteresis (Figure 21a,b) [13]. Interestingly, X-ray diffraction studies, carried out at 180 K, did not reveal any intermolecular connectivity for these two compounds. The bond distances of the coordination polyhedra at this temperature confirm a low-spin state for the iron(II) in both cases, which fits to the magnetic measurements.

The synthesis, characterization, magnetic properties and Mössbauer spectra of a linear iron(II) coordination chain of the formula  $[\text{Fe}^{\text{II}}(\text{1-bpp-ph-1-bpp})_n](\text{BF}_4)_{2n}$  (1-bpp-ph-1-bpp = 1,4-bis{2,6-bis(pyrazol-1-yl)pyridin-4-yl}benzene) has been reported [38]. The polynuclear structure of the complex was proven by an ESI mass spectrum in a methanol-DMF-acetonitrile solution, which also gives an evidence for the presence of a pentanuclear oligomeric unit  $[\text{Fe}_5^{\text{II}}(\text{1-bpp-ph-1-bpp})_5(\text{BF}_4)_8(\text{OH})_6]^{2+}$ , together with fragmented smaller nuclear entities. However, the only partial solubility of the complex in the above mentioned solvent mixture may give a hint for the presence of higher-chain homologues that possess even more than five repeating units. Considering the linear rod-like shape of the ligand, the formation of cyclic oligomers can be excluded (Figure 22).

A magnetic investigation of  $[\text{Fe}^{\text{II}}(\text{1-bpp-ph-1-bpp})_n](\text{BF}_4)_{2n}$  at variable temperature was carried out in the heating and cooling mode (Figure 22b). A thermal hysteresis with a 10 K loop width was observed, ( $T_{1/2}(\downarrow) = 318 \text{ K}$  and  $T_{1/2}(\uparrow) = 328 \text{ K}$ ), although the  $X_T$  value was almost constant below 225 K, reaching a minimum value of  $0.38 \text{ emu K mol}^{-1}$  at 4.5 K. This residual magnetic moment most likely comes from HS ions of the water end-capped iron(II) at the linear chain ends.

Another interesting family of iron(II) ST compounds with 2,6-bis(pyrazol-3-yl)pyridine ligands (Figure 19f) has been reported by Clemente-Leo'n et al. [39]. The complex consists of three heterometallic complexes, containing the ST cations  $[\text{Fe}^{\text{II}}(\text{3-bpp})]^{2+}$  and paramagnetic  $[\text{Cr}^{\text{III}}(\text{bpy})(\text{ox})]^-$  or  $[\text{Cr}^{\text{III}}(\text{phen})(\text{ox})]^-$  anions (bpy = 2,20-bipyridine, phen = phenanthroline, ox = oxalate) are described. Single-crystal X-ray structural analysis of the compound exhibits the formula  $[\text{Fe}^{\text{II}}(\text{3-bpp})_2][\text{Cr}^{\text{III}}(\text{bpy})(\text{ox})_2] \cdot 2\text{H}_2\text{O}$  and reveals two non-equivalent iron(II) sites, Fe(1A) and Fe(1B) (Figure 23a,b).

The Fe(1A)-N distances are in the range of 2.146(2)-2.210(2) Å and are characteristic for the HS configuration. On the contrary, the Fe(1B)-N distances are shorter, 1.921(2)-1.976(2) Å, and are typical

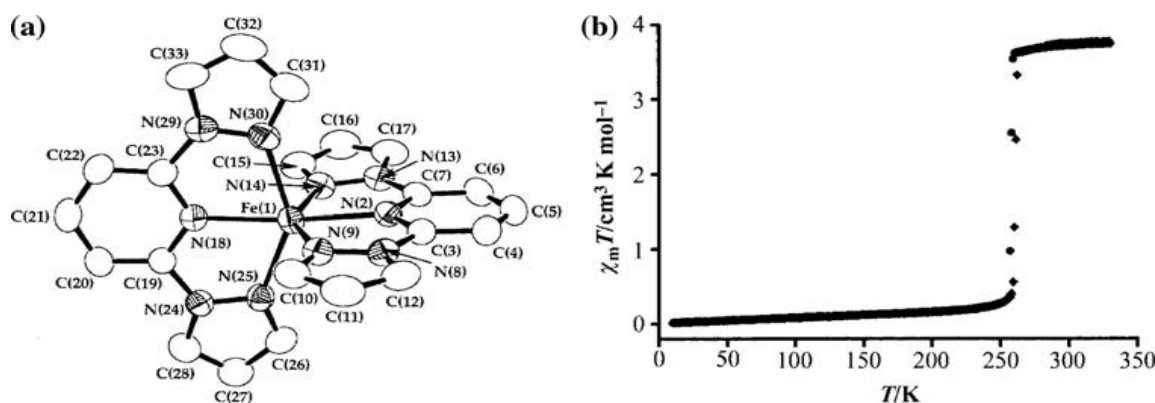
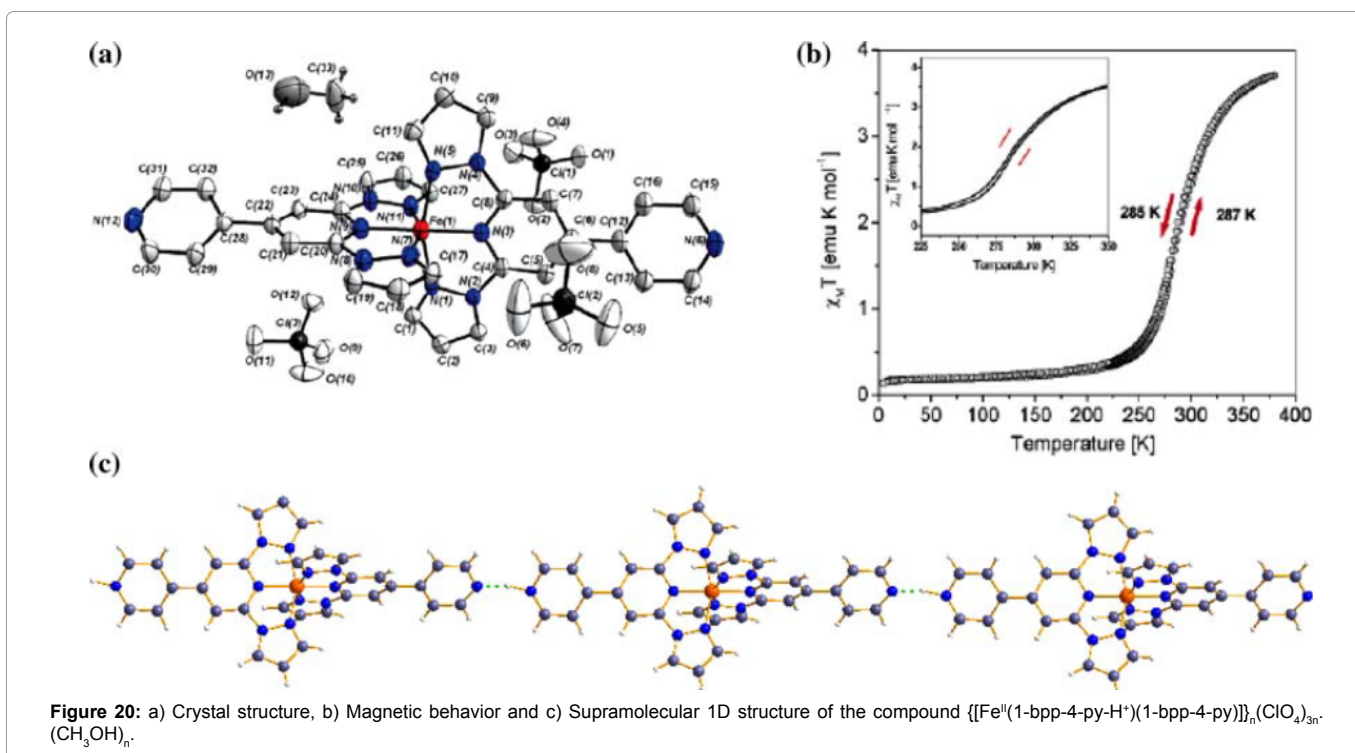
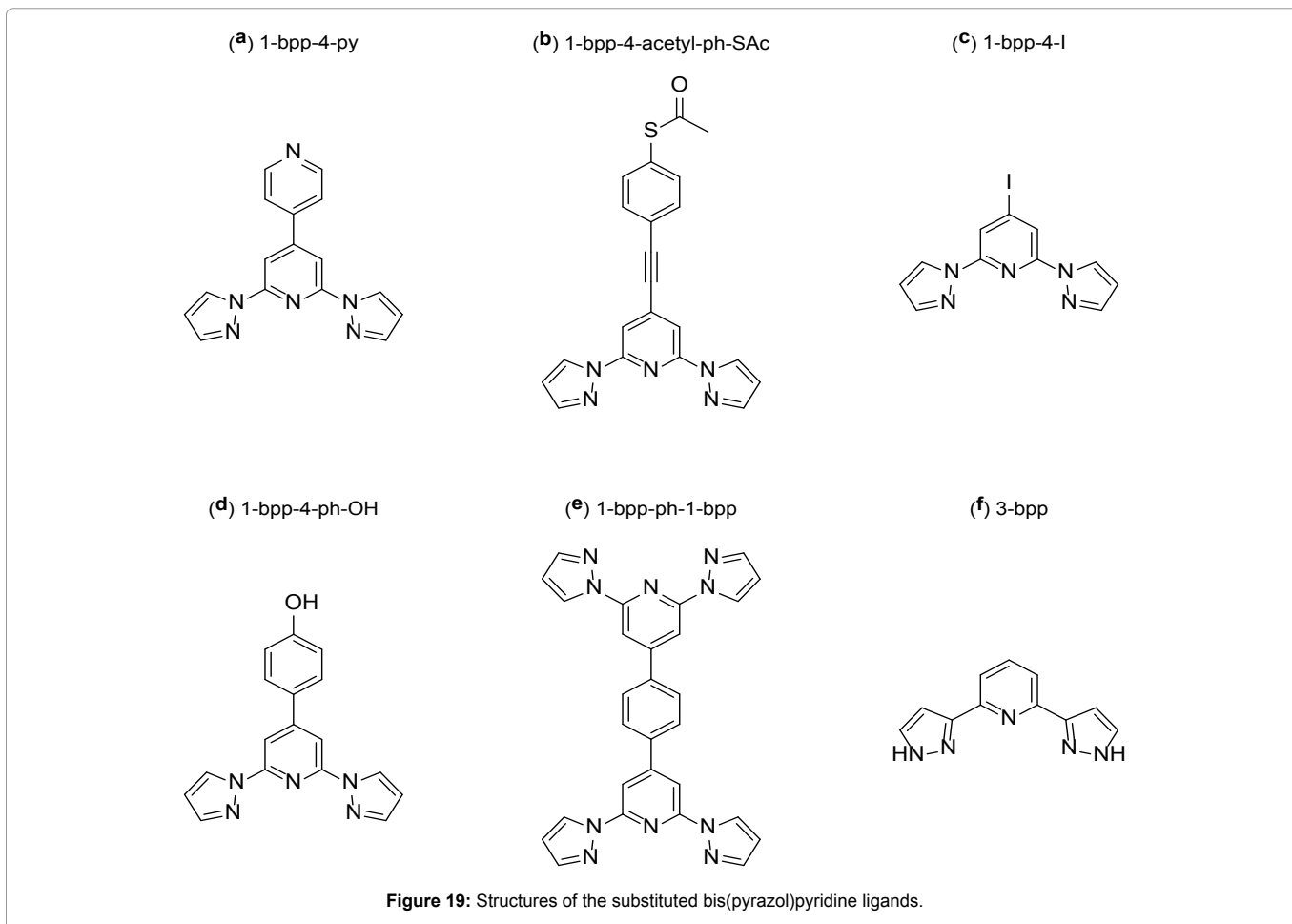
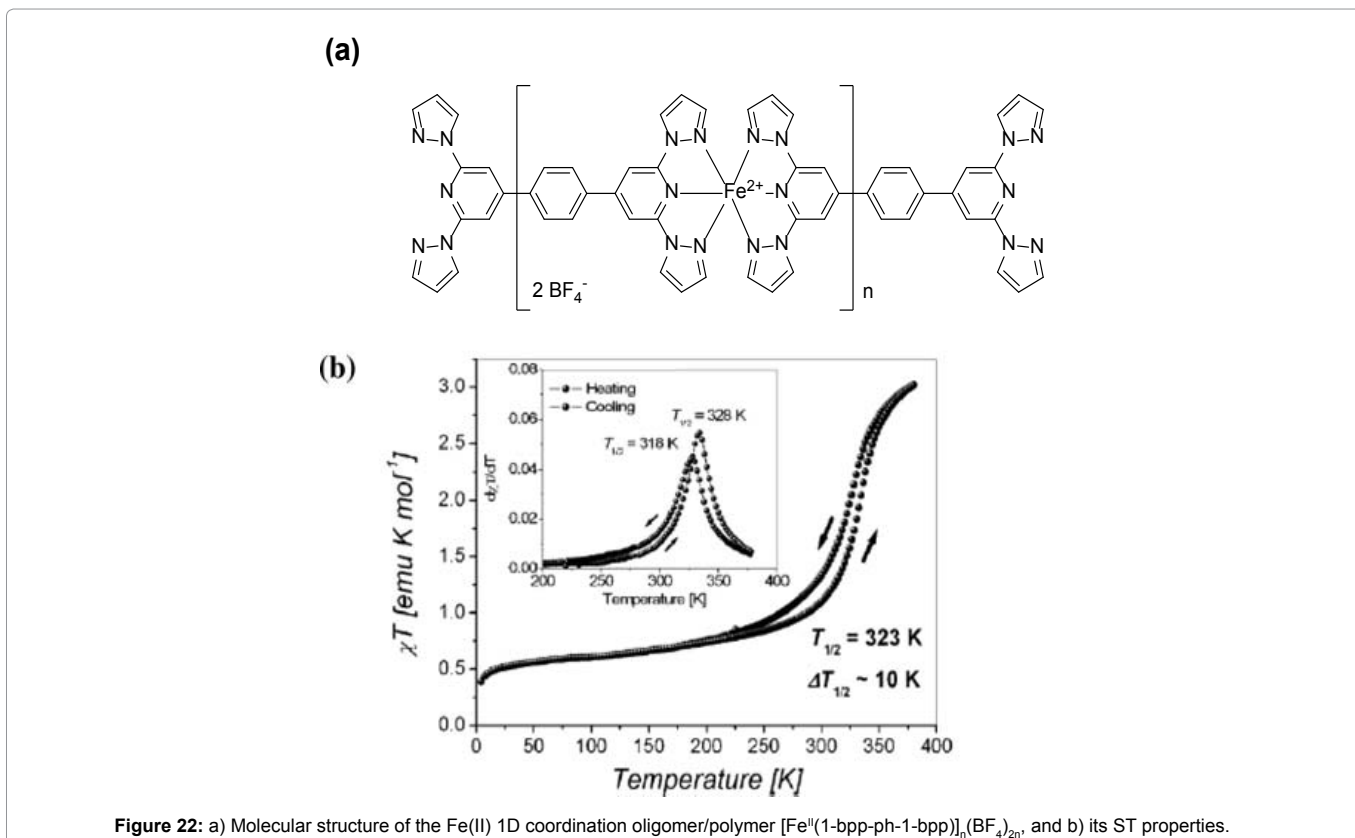
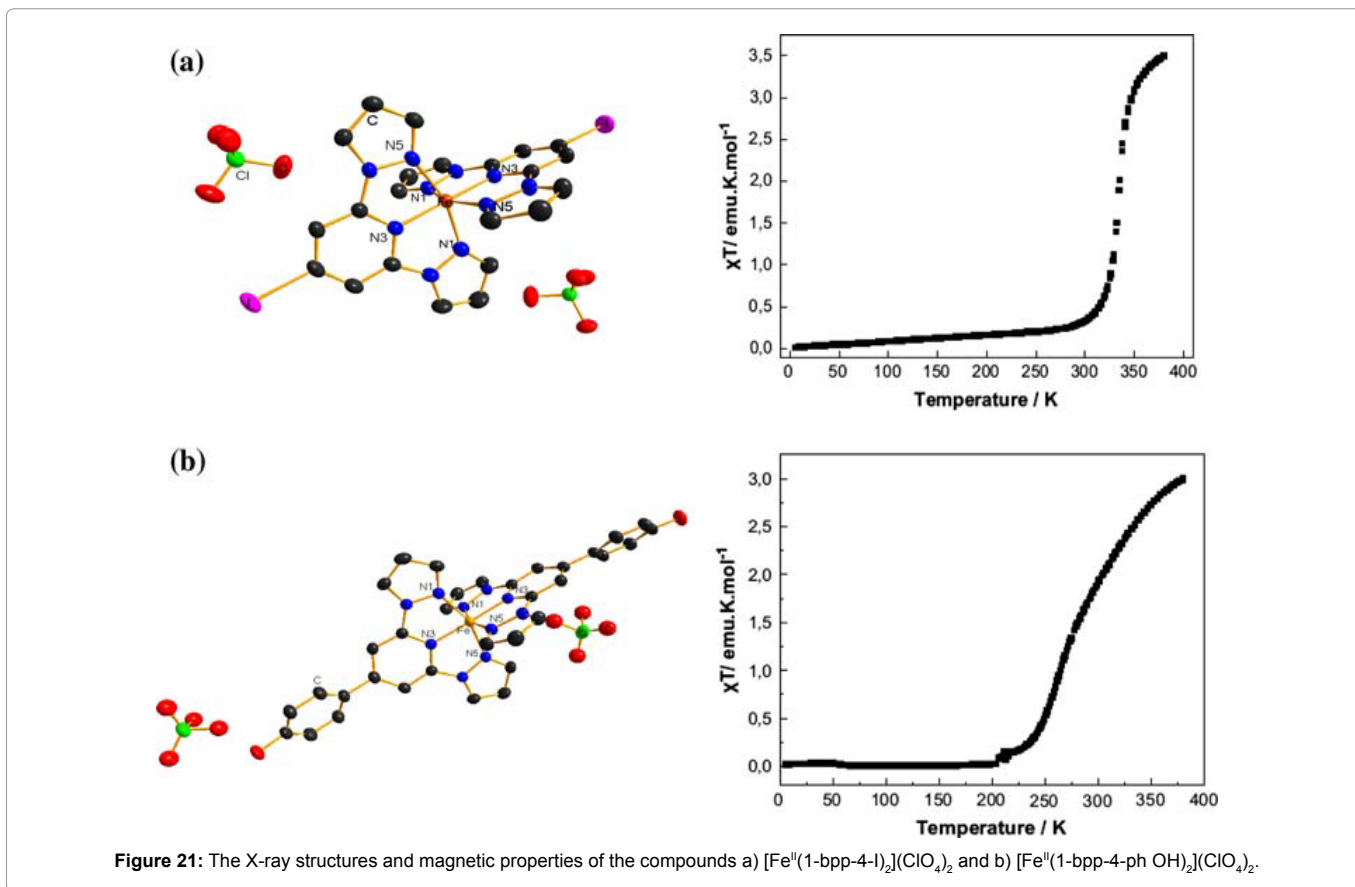


Figure 18: (a) Single-crystal structure and (b) magnetic properties of  $[\text{Fe}(\text{1-bpp})_2](\text{BF}_4)_2$ ,  $T_{1/2} = 259 \text{ K}$ ,  $\Delta T_{1/2} = 3 \text{ K}$ .





for LS iron(II). Thus, the structure shows the coexistence of HS and LS iron centers in the same crystalline phase. The four non-coordinating NH-groups of the center A have hydrogen-bonds to three anions  $[\text{Cr}^{\text{III}}(\text{bpy})(\text{ox})_2]^-$  and one water molecule, and the diamagnetic Fe(B) centers are surrounded by four  $[\text{Cr}^{\text{III}}(\text{bpy})(\text{ox})_2]^-$  anions with hydrogen-bonding distances. Due to the fact that the terminal O atoms of oxalates are better acceptors for hydrogen bonds than water, the electron density in the corresponding pyrazolyl ring of Fe(B) is increased with respect to the Fe(A) center, leading to a strengthening of the N(imine)-Fe(1B) bond, which favors the LS state for the Fe(1B) center. Additionally, one more type of intermolecular interaction was found in the supramolecular structure of this compound. The cationic  $[\text{Fe}^{\text{II}}(3\text{-bpp})]^{2+}$  units are organized into layers via  $\pi$ - $\pi$  stacking interactions between neighboring pyrazole parts (3.204 Å), and the anionic layers show aryl-aryl interactions between neighboring bispyridyl ligands (in the range 3.583(2)-3.742(1) Å). Finally, the cationic and anionic layers are interconnected by an intricate hydrogen-bonding network, involving water molecules. Note that dehydration and subsequent hydration are irreversible processes for this compound, and the crystal structure of the subsequent hydrated compound  $[\text{Fe}(3\text{bpp})_2][\text{Cr}^{\text{III}}(\text{bpy})(\text{ox})_2] \cdot 2\text{H}_2\text{O}$  exhibits only a HS type of the  $[\text{Fe}(3\text{-bpp})]^{2+}$  cation connected by hydrogen bonds to three  $[\text{Cr}^{\text{III}}(\text{bpy})(\text{ox})_2]^-$  anions and one molecule of water.

The magnetic properties of  $[\text{Fe}^{\text{II}}(3\text{-bpp})_2][\text{Cr}^{\text{III}}(\text{bpy})(\text{ox})_2] \cdot 2\text{H}_2\text{O}$  are shown in Figure 23c. The spin states of the iron(II) centers show a strong dependence on the presence of water molecules in the structure. The dehydrated compound shows a constant value of  $\chi^{\text{T}}$  (5.5 emu K mol<sup>-1</sup>) up to 320 K, which corresponds to the situation, where the Fe(A) centers are HS and the Fe(B) centers are in the LS state. Above 320 K, the  $\chi^{\text{T}}$  value decreases due to a removal of water molecules from the structure and then reaches a plateau at 7 emu K mol<sup>-1</sup> at 400 K, which corresponds to a 100% HS state for all iron(II) atoms. In the anhydrous sample, all iron(II) centers undergo reversible and reproducible STs with a 16 K thermal hysteresis loop centered above room temperature ( $T_{1/2}(\downarrow) = 353$  K and  $T_{1/2}(\uparrow) = 369$  K). In the second cycle, the hydrated material shows completely different magnetic behavior: below room temperature, the  $\chi^{\text{T}}$  value is constant (7.5 emu K mol<sup>-1</sup>) and in agreement with the spin-only value for a trinuclear system  $2\text{Cr}^{\text{III}} + \text{Fe}^{\text{II}}(\text{HS})$  ( $2X S_1 = 3/2 + S_2 = 4/2$ ,  $\chi^{\text{T}}$  spin-only = 6.76 emu K mol<sup>-1</sup>). Above 300 K, water is removed and the ST of the dehydrated compound is identical to that before

hydration. The authors also present two other compounds of the general formula  $[\text{Fe}^{\text{II}}(3\text{-bpp})_2][\text{Cr}^{\text{III}}(\text{phen})(\text{ox})_2] \cdot n\text{H}_2\text{O} \cdot m\text{CH}_3\text{OH}$ , where  $n = m = 1/2$ , which are isostructural with the previous complex. Again, the single crystal structure reveals two different iron(II) centers: Fe(A), which is HS and surrounded with three  $[\text{Cr}^{\text{III}}(\text{phen})(\text{ox})_2]^-$  complexes and one molecule of water; and Fe(B) centers, which are in the LS state and hydrogen bonded with four Cr<sup>III</sup>-complexes. There is also a similarity in terms of crystal packing: the  $\pi$ - $\pi$  interactions are in-between pyrazolyl rings (cation part) and in-between phenanthroline rings (anion part). Equally, only the solvent-free compounds exhibit a complete spin transition, which is situated above room temperature and accompanied by a thermal hysteresis ( $T_{1/2}(\downarrow) = 353$  K and  $T_{1/2}(\uparrow) = 369$  K,  $\Delta T_{1/2} = 4$  K).

Costa et al. [40] reported nonporous spin switching molecular materials, comprising of the Fe(II) complex of the formula  $[\text{Fe}(\text{bpp})(\text{H}_2\text{L})](\text{ClO}_4)_2 \cdot 1.5\text{C}_3\text{H}_6\text{O}$  (bpp = 2,6-bis(pyrazol-3-yl)pyridine,  $\text{H}_2\text{L} = 2,6\text{-bis}(5\text{-}(2\text{-methoxyphenyl})\text{pyrazol-3-yl})\text{pyridine}$ ) (Figure 24).

The Fe(II) complex occurs in its low spin state and crystallizes as compact discrete, nonporous material hosting acetone molecules in its crystal lattice. The system is able to extrude one third of lattice acetone and can switch to high spin state with a profound crystallographic change with the formula  $[\text{Fe}(\text{bpp})(\text{H}_2\text{L})](\text{ClO}_4)_2 \cdot \text{C}_3\text{H}_6\text{O}$  (1). The solvent extruded compound can be reversed to the original compound by a reabsorption of acetone.

The compound  $[\text{Fe}(\text{bpp})(\text{H}_2\text{L})](\text{ClO}_4)_2 \cdot \text{C}_3\text{H}_6\text{O}$  (2) can replace acetone by MeOH and H<sub>2</sub>O to form  $[\text{Fe}(\text{bpp})(\text{H}_2\text{L})](\text{ClO}_4)_2 \cdot 1.25\text{MeOH} \cdot 0.5\text{H}_2\text{O}$  (3). Besides all these transformations, all three Fe(II) complexes exhibit spin transition around room temperature (Figure 25).

**Miscellaneous room-temperature iron(II) ST systems:** Weber et al. [41] reported Jäger-type mononuclear iron(II) complexes.  $[\text{Fe}^{\text{II}}(\text{Ph}(\text{Imoxo})_2)(\text{HIm})_2]^{0+}$  ( $\text{Ph}(\text{Imoxo})_2 = \text{diethyl}(\text{E},\text{E})\text{-}2,2'\text{-}[1,2\text{-phenylenebis}(\text{iminomethylidene})]\text{-bis}[3\text{-butanoate}]$ , HIm = imidazole) (Figure 26a) was shown to exhibit an abrupt ST centered at approximately 297 K ( $T_{1/2}(\downarrow) = 244$  K and  $T_{1/2}(\uparrow) = 314$  K) and an unusually large thermal hysteresis loop with  $\Delta T_{1/2} = 70$  K (Figure 26b).

The HS value of the  $\chi^{\text{T}}$  product was found to be 3.32 emu K mol<sup>-1</sup> (at 325 K), which is in accordance to the pure Fe<sup>II</sup> HS state. The HS plateau remains approximately constant until 250 K, where an abrupt transition to the LS state is observed and its value  $\chi^{\text{T}}$  is 0.15 K (at

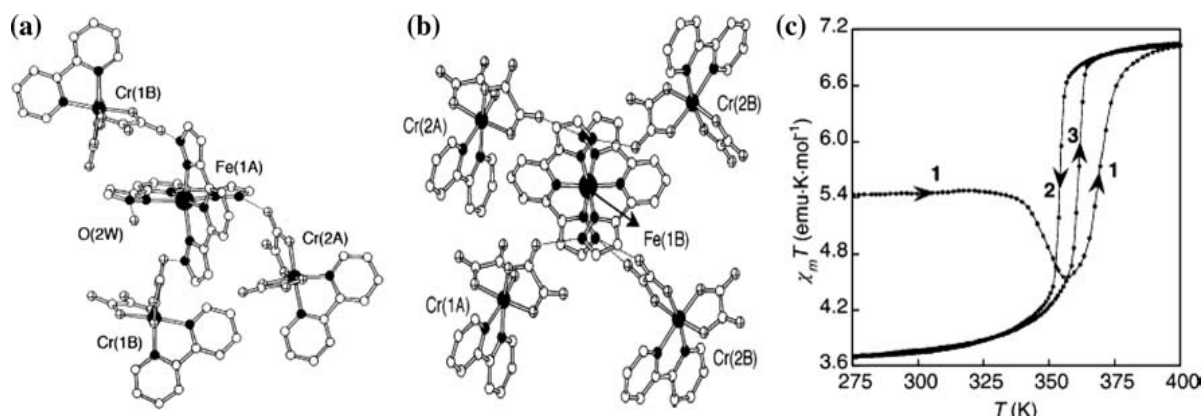


Figure 23: a) X-ray structure of  $[\text{Fe}^{\text{II}}(3\text{-bpp})_2][\text{Cr}^{\text{III}}(\text{bpy})(\text{ox})_2] \cdot 2\text{H}_2\text{O}$ , showing a two nonequivalent Fe(II) centers: the HS Fe<sup>II</sup> center (A) is linked by hydrogen bonds to three anions of  $[\text{Cr}^{\text{III}}(\text{bpy})(\text{ox})_2]^-$  and to one molecule of water; b) The LS Fe<sup>II</sup>(B) is connected by hydrogen bonds to four Cr<sup>III</sup> counter anions; c)  $\chi_m T$  versus T plot of  $[\text{Fe}^{\text{II}}(3\text{-bpp})_2][\text{Cr}^{\text{III}}(\text{bpy})(\text{ox})_2] \cdot 2\text{H}_2\text{O}$ ; heating of the hydrated compound (first step), cooling (second step) and heating (third step).

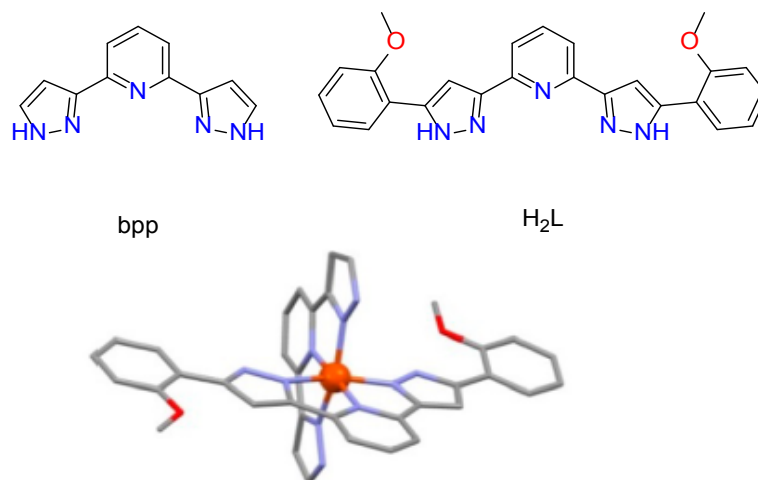


Figure 24: Ligands bpp and H<sub>2</sub>L (top) and structure of the cation [Fe(bpp)(H<sub>2</sub>L)]<sup>2+</sup>. Orange: Fe; red: O; purple: N; gray: C. Hydrogen atoms are not shown.

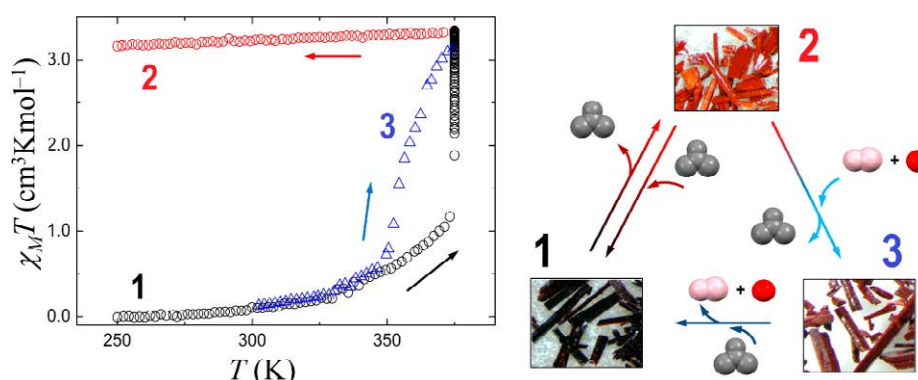


Figure 25:  $\chi_M T$  versus T (plot of the compound 1,2&3).

200 K). Upon heating, the LS state of [Fe<sup>II</sup>(Ph(Imoxo)<sub>2</sub>)(HIm)<sub>2</sub>]<sup>0</sup> stays constant up to 300 K (0.31 emu K mol<sup>-1</sup>), when it increases abruptly to the HS value. These ST properties are resistant to grinding effects and are fully reproducible

The single-crystal X-ray structure (Figure 26a) of [Fe<sup>II</sup>(Ph(Imoxo)<sub>2</sub>)(HIm)<sub>2</sub>]<sup>0</sup> was obtained at 275 K and the bond distances of the coordination polyhedron (Fe<sup>II</sup>-N(L) = 2.08 Å; Fe<sup>II</sup>-N(HIm) = 2.22 Å; Fe<sup>II</sup>-O = 2.03 Å) are in accordance to those, reported for similar HS iron(II) complexes. Due to the unusually large hysteresis, a detailed investigation of the intermolecular interactions is important for the understanding of the ST properties of this complex. A closer look at the supramolecular interactions between the mononuclear units reveals two different types of hydrogen bonds: The first one involves the NH hydrogen atom of the imidazole unit and the OCOEt oxygen atom (O<sub>5</sub>) of the ligand Ph(Imoxo)<sub>2</sub> (N...O = 2.841 Å), while the second connection is formed by the NH hydrogen atom of the second imidazole with the coordinated carbonyl oxygen atom (O<sub>1</sub>) of the ligand (Ph(Imoxo)<sub>2</sub>) (N...O = 2.83 Å). The combination of the two hydrogen-bond types leads to an infinite two-dimensional layer of linked mononuclear molecules. In addition, two other short contacts between the OCOEt oxygens and the aromatic C-H groups of the imidazole and phenylene rings seem to play an important role. This hydrogen-bond/short-contact network is clearly responsible

for the highly cooperative character of the ST, observed in this compound. It is interesting to note that a very similar mononuclear iron(II) complex involving the same ligands but a slightly different stoichiometry, [Fe<sup>II</sup>((Ph(Imoxo)<sub>2</sub>)(HIm)<sub>1.8</sub>)<sup>0</sup>, exhibits an ST above room temperature with a 4 K hysteresis, T<sub>1/2</sub>(↓) = 328 K and T<sub>1/2</sub>(↑) = 332 K [42]. The slight difference in stoichiometry seems to significantly disturb the subtly balanced H-bond network, leading to reduced cooperative interactions.

Another family of ST complexes, of the general formula [Fe<sup>II</sup>(L)<sub>2</sub>](X)<sub>2</sub>·nS, has been reported by Boča et al. [43-46], where L are tridentate N-donor benzimidazole-type ligands (Figure 27).

The magnetic properties of [Fe<sup>II</sup>(bzimpy)<sub>2</sub>](BPh<sub>4</sub>)<sub>2</sub>·nH<sub>2</sub>O show a strong dependence on the presence of water in the lattice (n = 4, 2, 0) [46]. The complex with n = 4 exhibits a spin transition in the temperature range of 280–350 K. The μ<sub>eff</sub> values in the LS (ca 1.6 μB) and HS (ca 5.5 μB) states are typical of the S = 0 ↔ 2 spin crossover. Up to 323 K, the spin transition occurs without thermal hysteresis and is reproducible (Figure 28). Above 400 K, the complex loses water and stays in its HS state.

The perchlorate analogue [Fe<sup>II</sup>(bzimpy)<sub>2</sub>](ClO<sub>4</sub>)<sub>2</sub>·0.25H<sub>2</sub>O shows an abrupt spin transition centered above RT, T<sub>1/2</sub>(↓) = 409 K and T<sub>1/2</sub>(↑) = 397 K (Figure 29b); the hysteresis width is ΔT<sub>1/2</sub> = 12 K

[45]. In this compound, a  $\pi$ - $\pi$  stacking 3D network exists among the benzene rings, which probably causes and/or enhances the solid-state cooperativeness. At the transition temperature, the complex shows a reversible, first-order phase transition (as verified by DSC calorimetry) and exhibits a structural phase transition (as seen in the powder diffraction patterns).

The compound  $[\text{Fe}^{\text{II}}(\text{tzimpy})_2](\text{ClO}_4)_2 \cdot 2\text{H}_2\text{O}$  shows a strong temperature dependence of the effective magnetic moment, leading to the conclusion that the ST occurs above room temperature (Figure 30) [45]. Values of  $\mu_{\text{eff}}$  are  $1.0 \mu\text{B}$  below 250 K (LS) and  $5.1 \mu\text{B}$  at 385 K (HS), which means that a ST occurs between the spin states  $S = 0$

and 2. This ST is associated with a thermal hysteresis, centered at  $T_{1/2} = 323 \text{ K}$  ( $T_{1/2}(\downarrow) = 306 \text{ K}$ ,  $T_{1/2}(\uparrow) = 340 \text{ K}$ ), and the hysteresis width is  $\Delta T_{1/2} = 35 \text{ K}$ .

The neutral, mononuclear iron(II) complex of formula  $[\text{Fe}^{\text{II}}(\text{bzimpy}_{-1\text{H}})_2] \cdot \text{H}_2\text{O}$  with the deprotonated ligand bzimpy-1H shows a more complex magnetic behavior (Figure 31). The effective magnetic moment rises from its room-temperature value of  $1.3 \mu\text{B}$  at 500 K. Around this temperature, the compound undergoes irreversible changes: Elimination of the crystal water, a color change (blue-green), followed by a structural change (as determined by TGA analysis, IR spectroscopy and X-ray powder diffraction

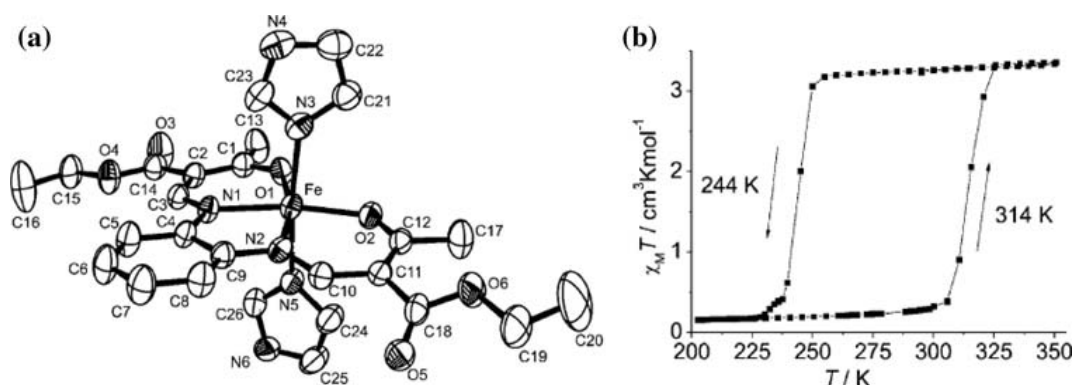


Figure 26: a) Single-crystal X-ray structure of the complex  $[\text{Fe}^{\text{II}}((\text{Ph}(\text{Imoxo})_2))(\text{HIm})_2]_0$ , b) ST behavior, with a thermal hysteresis  $\text{DT} = 70 \text{ K}$ .

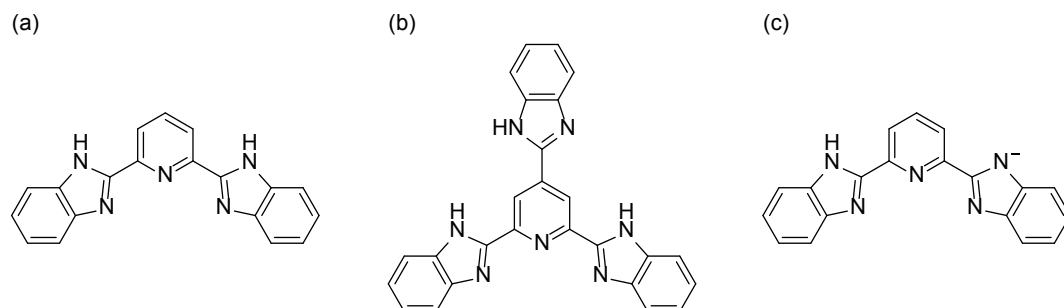


Figure 27: Structure of the benzimidazole-type ligands: a) bzimpy, 2,6-bis(benzimidazol-2-yl)pyridine; b) tzimpy, 2,4,6-tris(benzimidazol-2-yl)pyridine; c) bzimpy-1H, mono-deprotonated bzimpy.

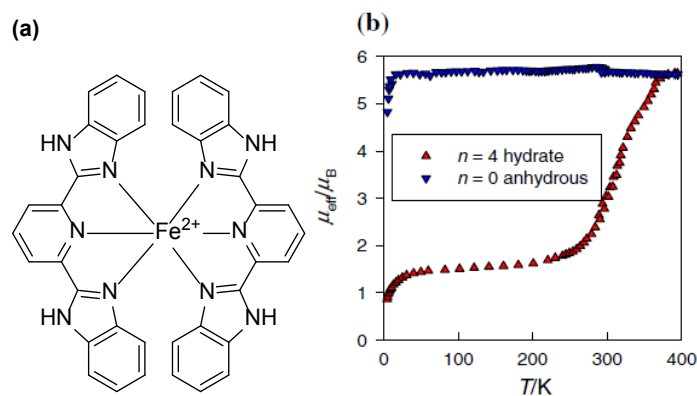
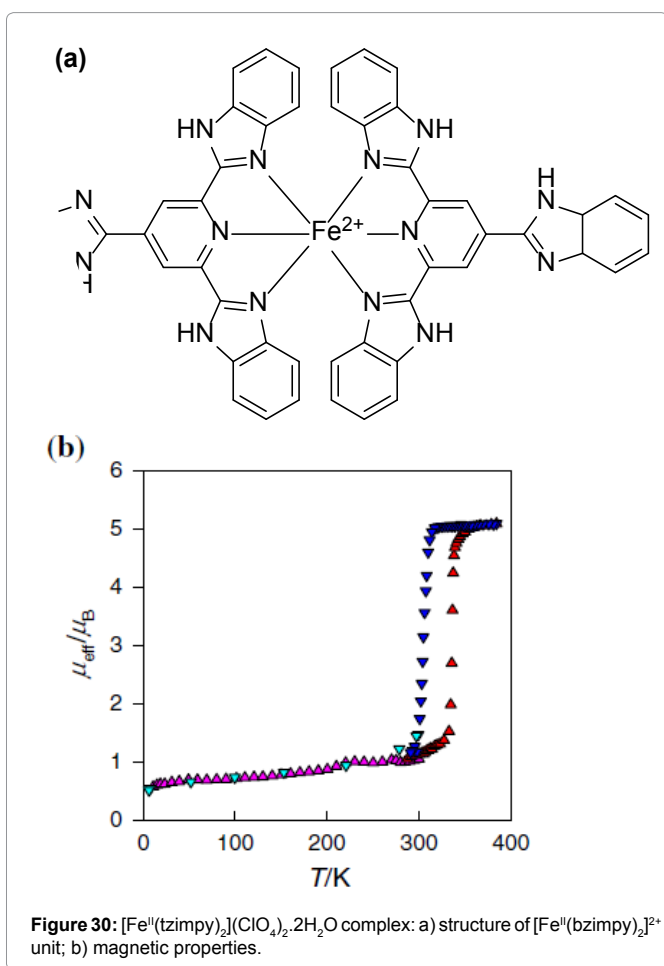
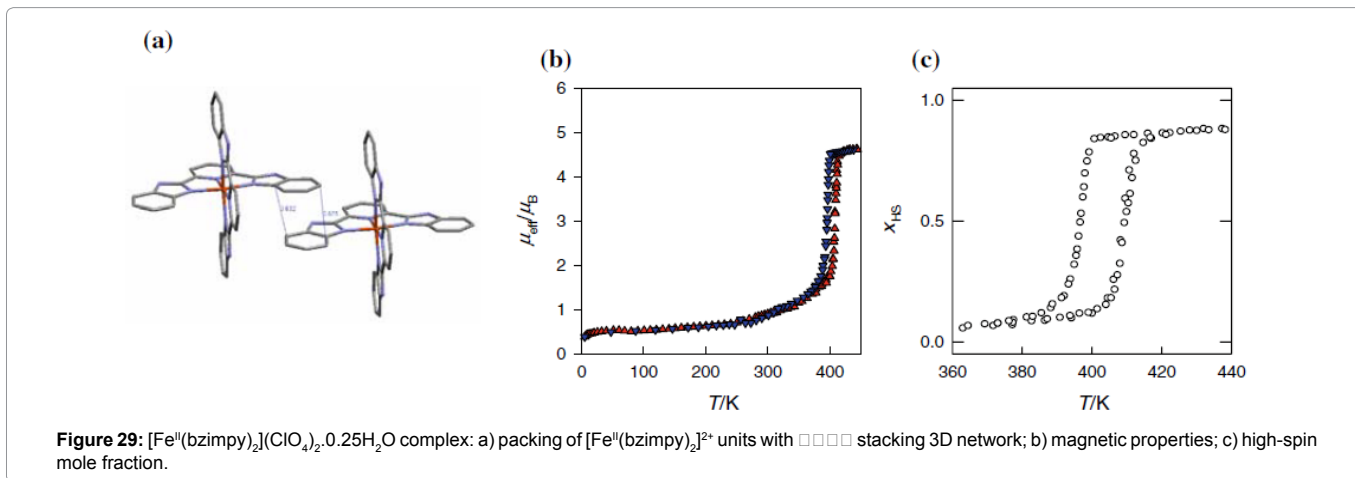


Figure 28:  $[\text{Fe}(\text{bzimpy})_2](\text{BPh}_4)_2 \cdot n\text{H}_2\text{O}$  complexes: a) structure of  $[\text{Fe}(\text{bzimpy})_2]^{2+}$ ; b) magnetic properties.



measurements). After that, in the cooling mode, the  $\mu_{\text{eff}}$  gradually decreases and below 300 K, it reaches the value 2.0  $\mu\text{B}$ . This value is caused by partial oxidation of the complex above 500 K (the presence of iron(III) in the sample was confirmed by Mössbauer spectroscopy).

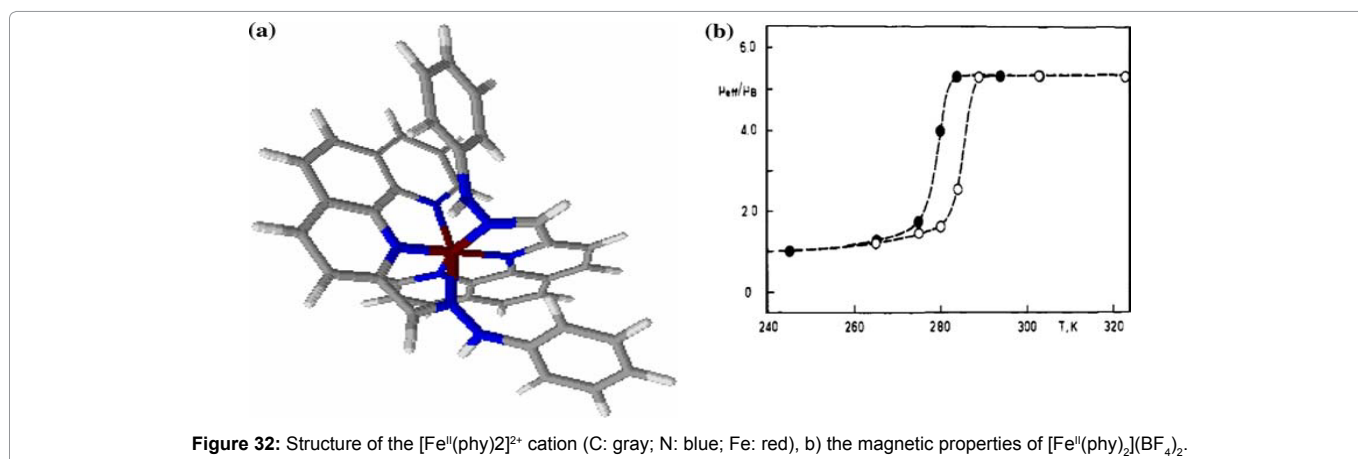
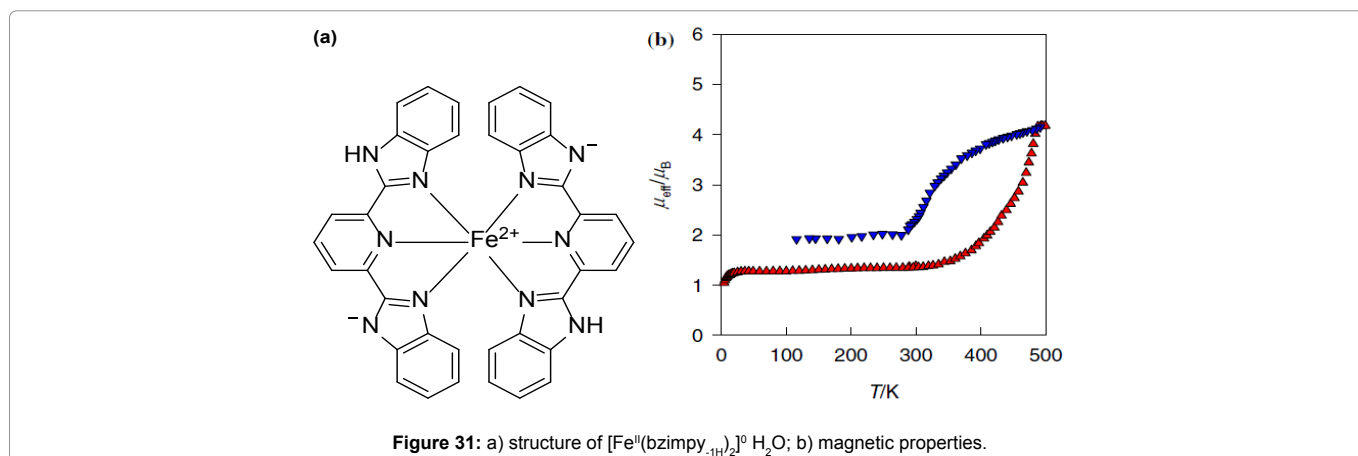
There is another family of mononuclear iron(II) complexes of the bidentate N-donor ligand 2-(2'-pyridyl)benzimidazole (pyben) [47]. In this work, six complexes of the general formula [Fe<sup>II</sup>(pyben)<sub>3</sub>](X)<sub>2</sub>·nH<sub>2</sub>O are described. ST around room-temperature are observed for

X = BPh<sub>4</sub><sup>-</sup>, n = 1; X = Cr(NH<sub>2</sub>)(NCS)<sub>4</sub><sup>-</sup>, n = 0 and X = BF<sub>4</sub><sup>-</sup>, n = 2. However, due to experimental limitations, magnetic measurements of these compounds were only carried out at temperatures up to room temperature, which means that their STs were incomplete.

The ST properties of the compound [Fe<sup>II</sup>(phy)<sub>2</sub>](BF<sub>4</sub>)<sub>2</sub> (phy = 1,10 phenanthroline-2-carbaldehyde phenylhydrazone) (Figure 32a) are reported in several papers by König et al. [48-50]. Magnetic measurements (Figure 32b) of this complex reveal a ST,  $T_{1/2}(\downarrow) = 279$  K and  $T_{1/2}(\uparrow) = 286$  K, that exhibits a hysteresis loop of  $\Delta T_{1/2} = 7$  K. This thermal hysteresis is confirmed by other techniques: Mössbauer spectroscopy ( $T_{1/2}(\downarrow) = 277$  K and  $T_{1/2}(\uparrow) = 286$  K), variable-temperature X-ray powder diffraction ( $T_{1/2}(\downarrow) = 277$  K and  $T_{1/2}(\uparrow) = 284$  K) and DSC studies ( $T_{1/2}(\downarrow) = 276$  K and  $T_{1/2}(\uparrow) = 288$  K). The same group also presented a very detailed analysis of the hysteresis of this complex [49] and the effect of pressure on the thermal hysteresis [50].

Among the group of mononuclear iron(II) room-temperature ST compounds, we should mention the complexes of the formula [Fe<sup>II</sup>(TRIM)<sub>2</sub>](X)<sub>2</sub>·MeOH (X = Br<sup>-</sup>, HCO<sub>2</sub><sup>-</sup>; TRIM = 4-(4-imidazole-methyl)-2-(2-imidazolylmethyl) imidazole) [51]. Both compounds exhibit very similar magnetic properties - the magnetic moments start to increase around 250 K from the low spin state, and at 380 K, they reach 5.1  $\mu\text{B}$  (X = Br<sup>-</sup>) and 5.0  $\mu\text{B}$  (X = HCO<sub>2</sub><sup>-</sup>) respectively (the ST is not finished at this temperature). The transition temperatures were determined to be  $T_{1/2} = 340$  K for the Br<sup>-</sup> and  $T_{1/2} = 330$  K for the HCO<sub>2</sub><sup>-</sup> analogue. The absence of thermal hysteresis seems to be a characteristic for this kind of compounds.

The crystal structure of the binuclear complex [(TPyA)Fe<sup>II</sup>(DBQ<sup>2-</sup>)Fe<sup>II</sup>(TPyA)](BF<sub>4</sub>)<sub>2</sub> (TPyA = tris(2-pyridylmethyl)amine; H<sub>2</sub>DBQ = 2,5-di-t-butyl-3,6-dihydroxy-1,4-benzoquinone) elucidates strong  $\pi$ - $\pi$  interactions between the iron(II) dimers, which may indicate a two dimensional sheet structure [52]. The pyridyl groups of the TPyA ligand and the benzene ring of the DBQ<sup>2-</sup> ligand are involved in C-H- $\pi$  and offset face-to-face  $\pi$ - $\pi$  interactions between the iron(II) dimers. The X-ray crystal structure of this compound (Figure 33a) was measured at 208 K and indicates that both iron(II) ions are in their LS state. At 298 K, the bond distances indicate a mixed spin state in the crystal, higher than observed for the LS state, but smaller than observed for typical HS ions. These results agree with the results of the magnetic measurements at variable temperature in a good way (Figure 33b). The magnetic moment starts to increase from an LS value of around 200 K, reaching 6.69  $\mu\text{B}$  at 380 K, which is very close



to the spin-only value of the system  $2 \uparrow 9 \downarrow S = 2$  (ca.  $6.93 \mu\text{B}$ ).

Boilot et al. [53] reported the synthesis, characterization and magnetic investigation of  $\text{Fe}^{\text{II}}$  complexes of the Schiff base ligands derived from pyridine-2-carbaldehyde with 2-hydroxy-5-nitroaniline (Hpap-5 $\text{NO}_2$ ) and 5-nitro-salicylaldehyde with quinolin-8-amine, respectively (Hqsal-5 $\text{NO}_2$ ) (Figure 34).

The complexes are of the formulae  $\text{Fe}(\text{pap-5NO}_2)_2$ ,  $\text{Fe}(\text{qsal-5NO}_2)_2$  and  $\text{Fe}(\text{qsal-5NO}_2)_2 \cdot 2\text{H}_2\text{O}$  (Figure 35). The structures of these complexes include the  $[\text{N}_4\text{O}_2]$  asymmetrical environment of  $\text{Fe}(\text{II})$ , chelated by five or six membered rings. The  $\text{NO}_2$ -groups of the ligands are located close to the aromatic planes. At 100K the bond lengths  $\text{Fe}-\text{N}_1 = 1.9570(19)$  and  $\text{Fe}-\text{N}_2 = 1.8841(16)$  are shorter,  $1.921(2)-1.976(2) \text{ \AA}$ , and are typical for iron (II) in its LS state.

The spin crossover properties of the compounds  $\text{Fe}(\text{pap-5NO}_2)_2$  and  $\text{Fe}(\text{qsal-5NO}_2)_2 \cdot \text{H}_2\text{O}$  were measured with crystalline powders in a range of 10-400 K. An abrupt spin transition, centered at room temperature with a hysteresis of 17K, occurs for the former, while the latter shows a gradual spin crossover above 300K (Figure 36).

Synthesis, characterization and spin crossover properties of  $\text{Fe}(\text{II})$  complexes of the Schiff base ligand derived from 1H-imidazole-4-carbaldehyde and 2-aminobenzhydrazide have been reported by Wu et al. [54] (Figure 37).

The complexes are of the formulae  $[\text{Fe}(\text{Liq})_2](\text{BF}_4)_2 \cdot (\text{CH}_3\text{CH}_2)_2\text{O}$  and  $[\text{Fe}(\text{Liq})_2](\text{BF}_4)_2 \cdot 3\text{H}_2\text{O}$  (Figure 38). The ligand Liq coordinates to

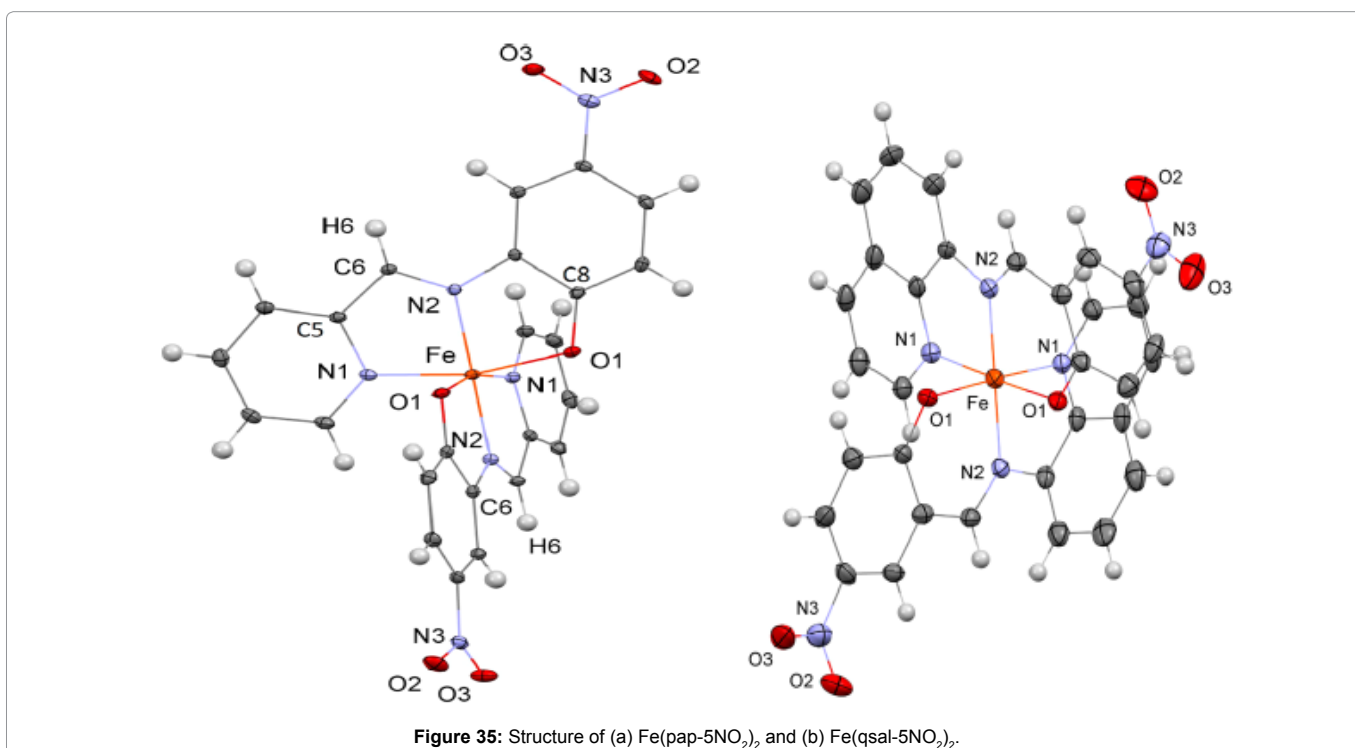
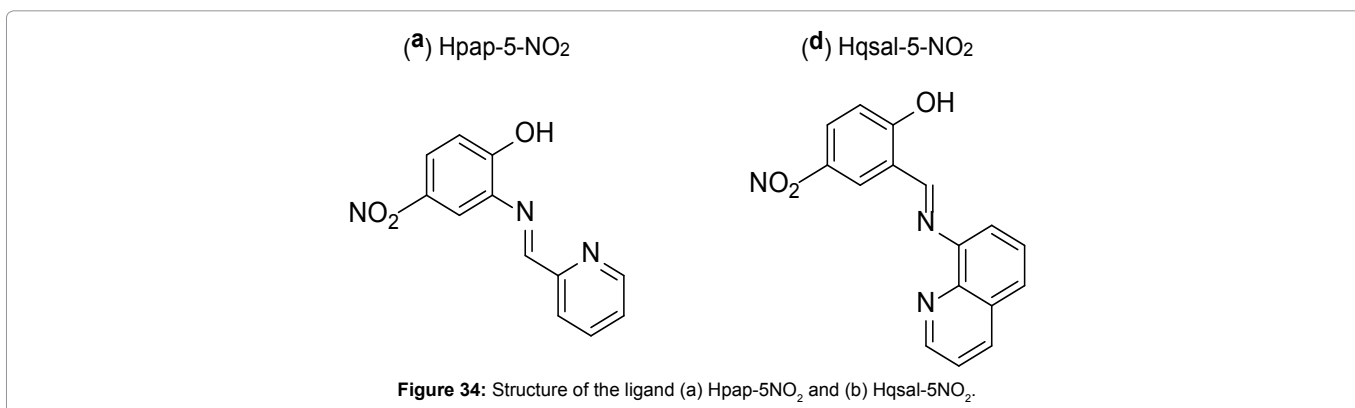
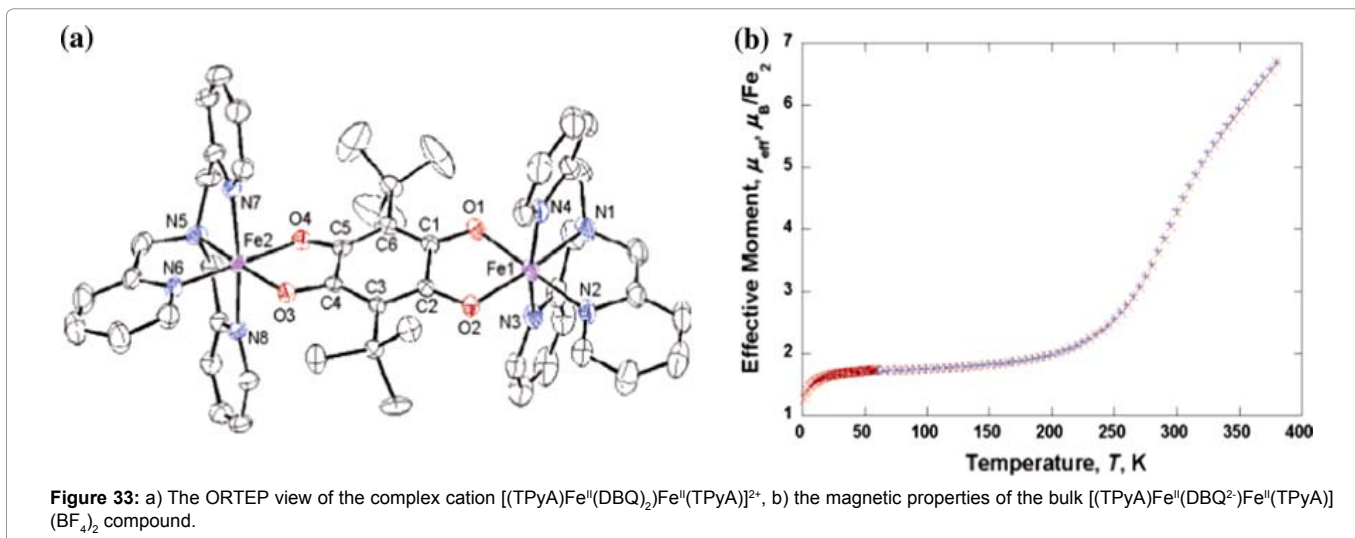
the  $\text{Fe}(\text{II})$  center equatorially through two imidazole nitrogens and axially by to the imine nitrogen atom. The  $\text{BF}_4^-$  remain as the counter anion. The single crystal to single crystal solvation transformation and the influence on the crystal structures and the magnetic hysteresis were investigated in an etherification-hydration cycle.

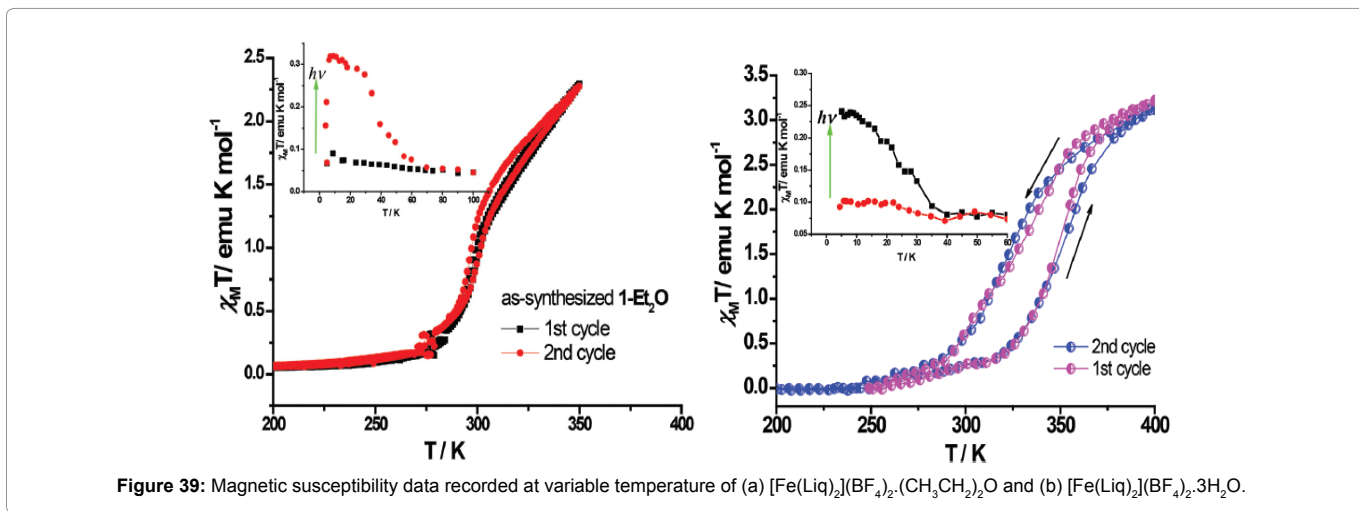
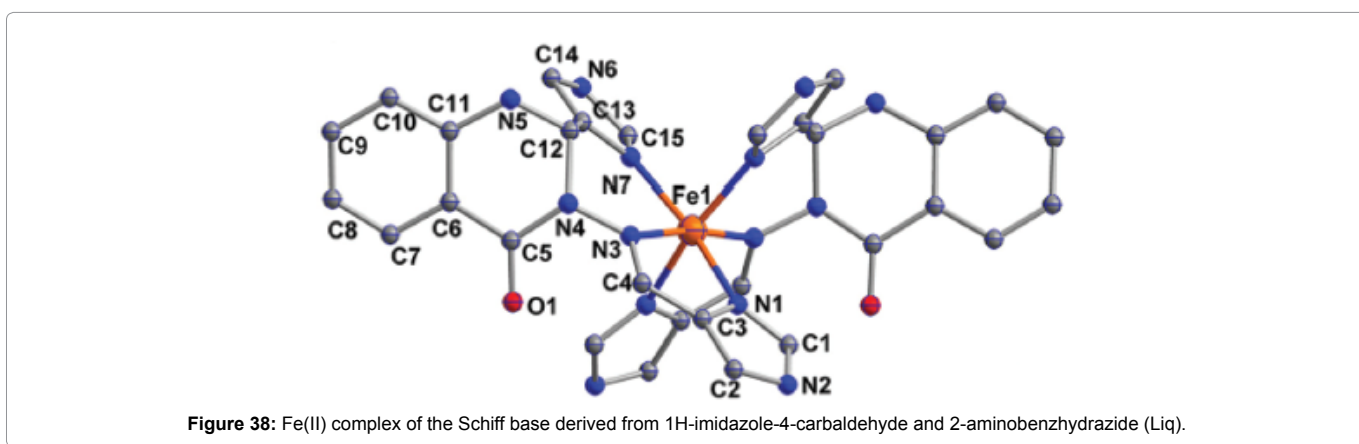
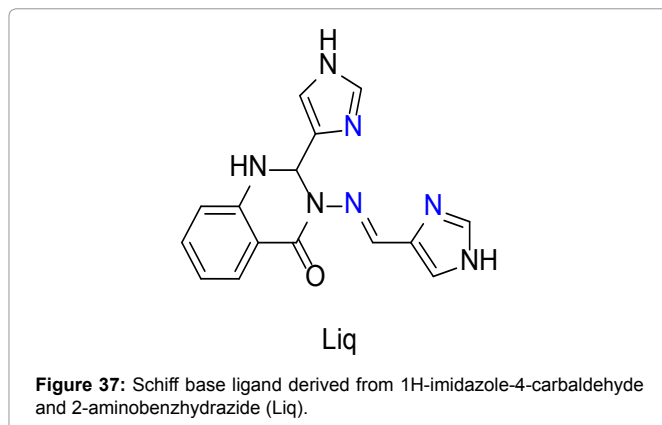
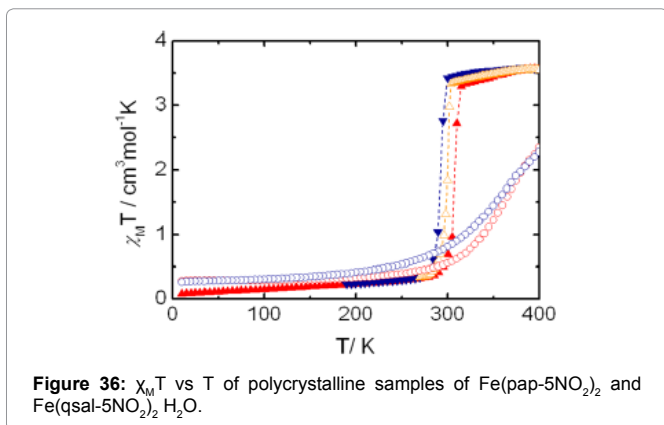
The etherified phase exhibits a spin crossover at room temperature ( $T_{1/2} = 305\text{K}$ ) with a negligible thermal hysteresis, however, the hydrated phase exhibit a spin transition around room temperature with an hysteresis loop ( $T_{1/2} \uparrow = 305\text{K}$  and  $T_{1/2} \downarrow = 326\text{K}$ ) (Figure 39).

Spin crossover properties of enantiomers, co-enantiomers, recemates and co-racemates of  $\text{Fe}(\text{II})$  complexes of the Schiff base derived from Phenylethylamine and 1-R-2-imidazolecarboxaldehyde ( $\text{R} = \text{C}_4\text{H}_9$  and  $\text{C}_5\text{H}_{11}$ ) (Figure 40) have been reported by Gu et al. [55].

Enantiomeric  $\text{Fe}(\text{II})$  complexes 4R, 4S, 5R and 5S of the general formulae  $[\text{Fe}(\text{L})_3]^{2+}$  have been synthesized (Figure 41). The crystal structure reveals that the central iron(II) is coordinated to six nitrogen atoms, two, each from the three ligands, generating a distorted octahedral geometry around the central metal ion. The average  $\text{Fe}-\text{N}$  bond lengths of 4R and 4S ( $2.204 \text{ \AA}$ ) are consistent with the values of an iron(II) ion in the HS state.

The binary co-crystallization of the prior synthesized enantiomers resulted in the spin crossover co-enantiomers 4R5R and 4S5S and the recemates 4RS and 5RS and the co-recemate 4RS5RS.





Magnetic studies at variable temperature reveal that 4R remains in the high spin state throughout the measured temperature range 2-400K. The compound 5R shows a steep spin transition at 291K and the co-enantiomers 4R5R and 4RS exhibit gradual spin transition at a higher temperature of 301K. The racemic alloys show spin transitions above room temperature with a hysteresis loop (Figures 42 and 43).

Weber et al. [56] reported the synthesis, characterization and magnetic investigations of mixed ligand 1D coordination polymers of iron (II) with the general formula  $[\text{FeL}(\text{pina})] \cdot x\text{Solvent}$  (where  $\text{L} = [([3,3']\text{-}1,2\text{-phenylenebis}(\text{iminomethylidene}))\text{bis}(2,4\text{-}$

pentanedionato)(2-)-N,N',O2,O2'] and  $\text{pina} = \text{N}(\text{pyrid-4-yl})\text{isonicotinamide}$ ) (Figure 44).

L acts as a tetradentate ligand coordinating through both, the azomethine nitrogens and oxygens of the Schiff base. Pina is acting as an axial bridging ligand, generating a 1D polymeric structure for the complex (Figure 45). The average values of the bond lengths are 1.90 Å ( $\text{Fe-N}_{\text{eq}}$ ), 1.94 Å ( $\text{Fe-O}_{\text{eq}}$ ) and 2.01 Å ( $\text{Fe-N}_{\text{ax}}$ ). The observed O-Fe-O angle is with 88.9° clearly indicative for iron(II) in its LS state. The axial pina ligand links the iron centers as bridging bidentate ligand, generating an infinite one-dimensional chain.

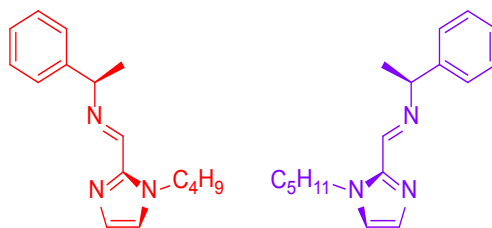


Figure 40: Structure of the Schiff base ligand derived from Phenylethylamine and 1-R-2-imidazolecarboxaldehyde (R = C<sub>4</sub>H<sub>9</sub> and C<sub>5</sub>H<sub>11</sub>).

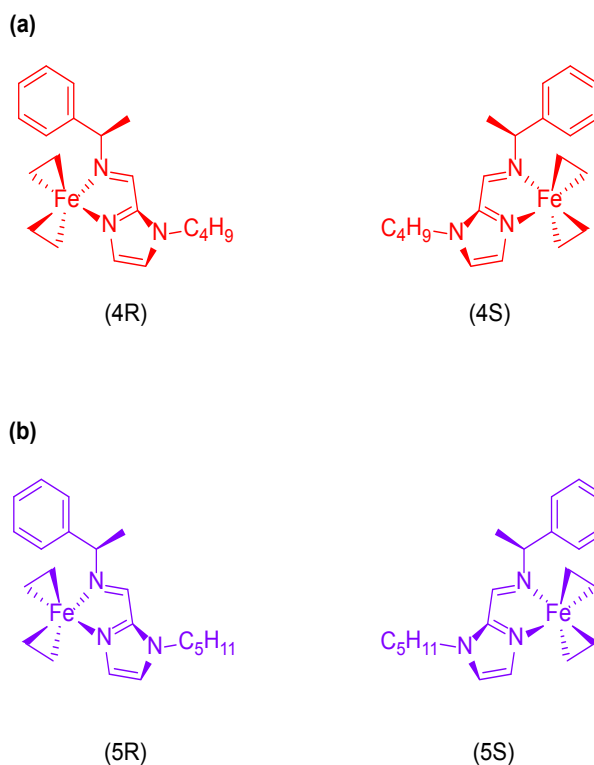


Figure 41: The structures of the enantiomeric forms of the Fe(II) complexes.

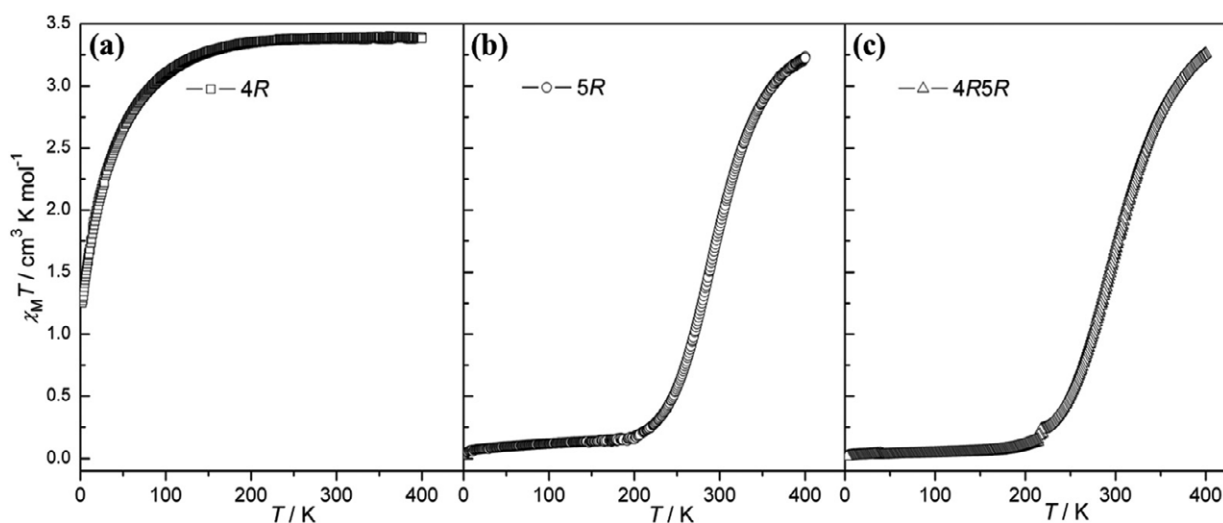


Figure 42:  $x_M T$  versus T for 4R(a), 5R(b) and 4R5R(c).

Magnetic studies at variable temperature (Figure 46) show that the crystalline sample of the composition  $[\text{FeL}(\text{pina})] \cdot x\text{H}_2\text{O}/\text{MeOH}$  exhibits a spin transition, centered around room temperature with a wide hysteresis loop of 88K ( $T_{1/2}^{\uparrow} = 328 \text{ K}$  and  $T_{1/2}^{\downarrow} = 240 \text{ K}$ ). For the single crystals of  $[\text{FeL}(\text{pina})] \cdot 2\text{MeOH}$  a spin transition with a 51 K hysteresis loop can be observed ( $T_{1/2}^{\uparrow} = 296 \text{ K}$  and  $T_{1/2}^{\downarrow} = 245 \text{ K}$ ).

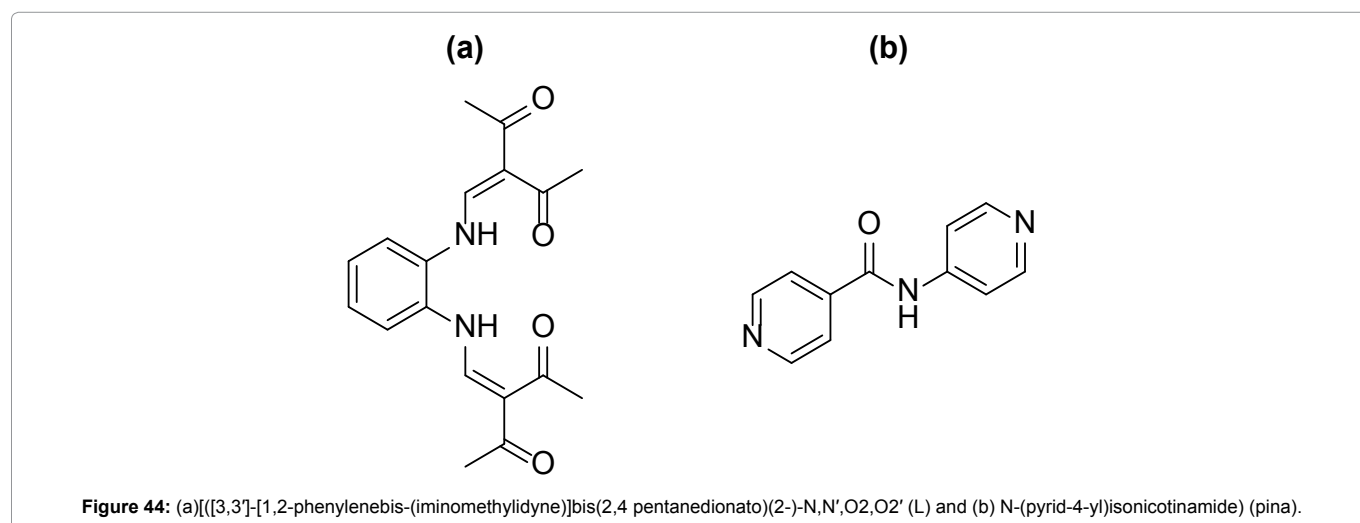
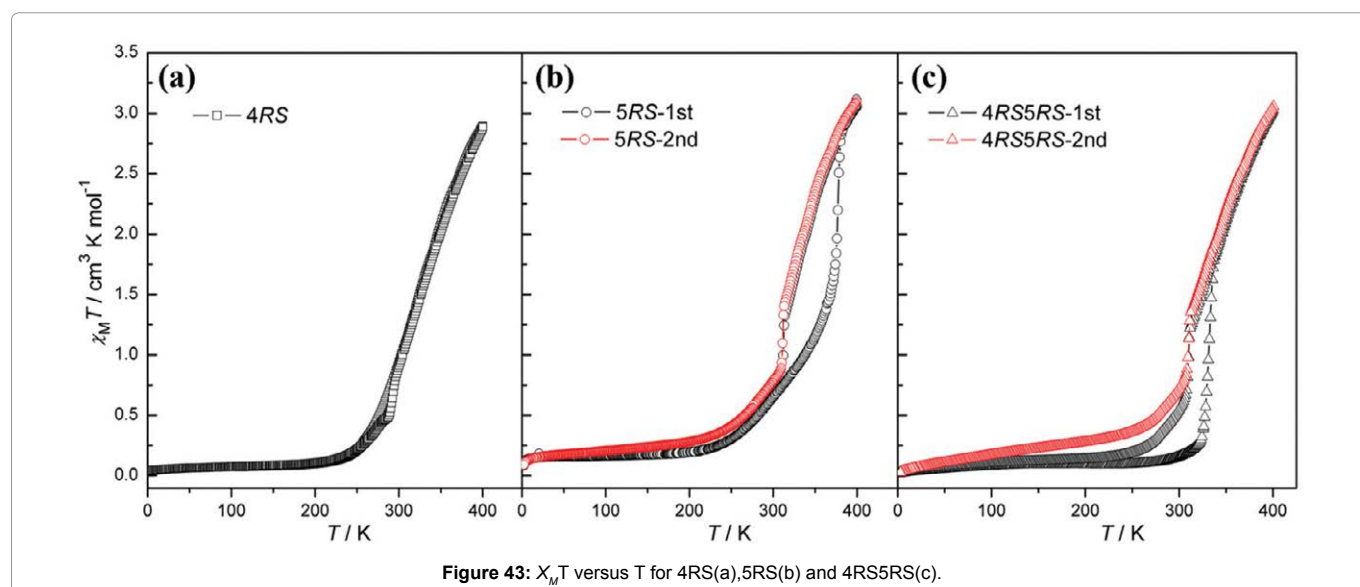
## Conclusion

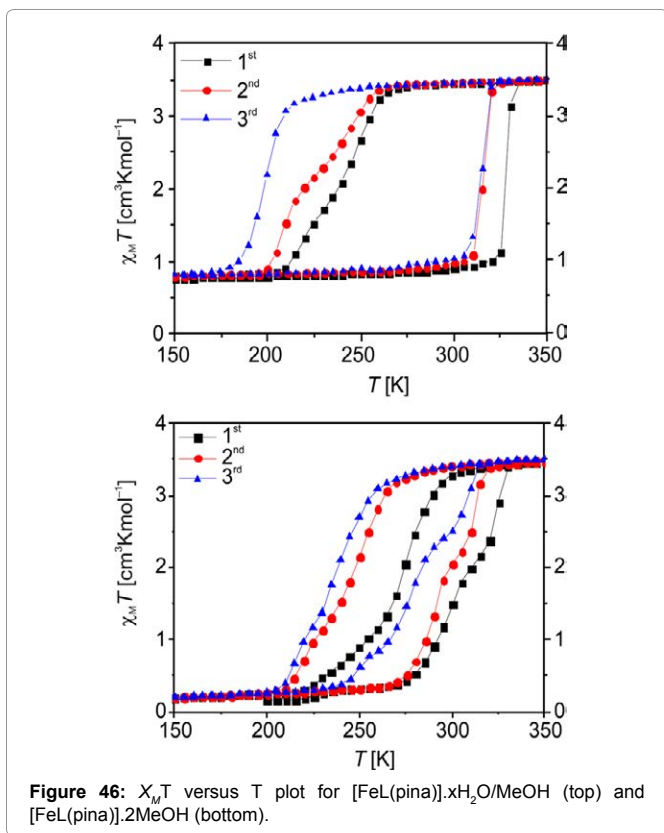
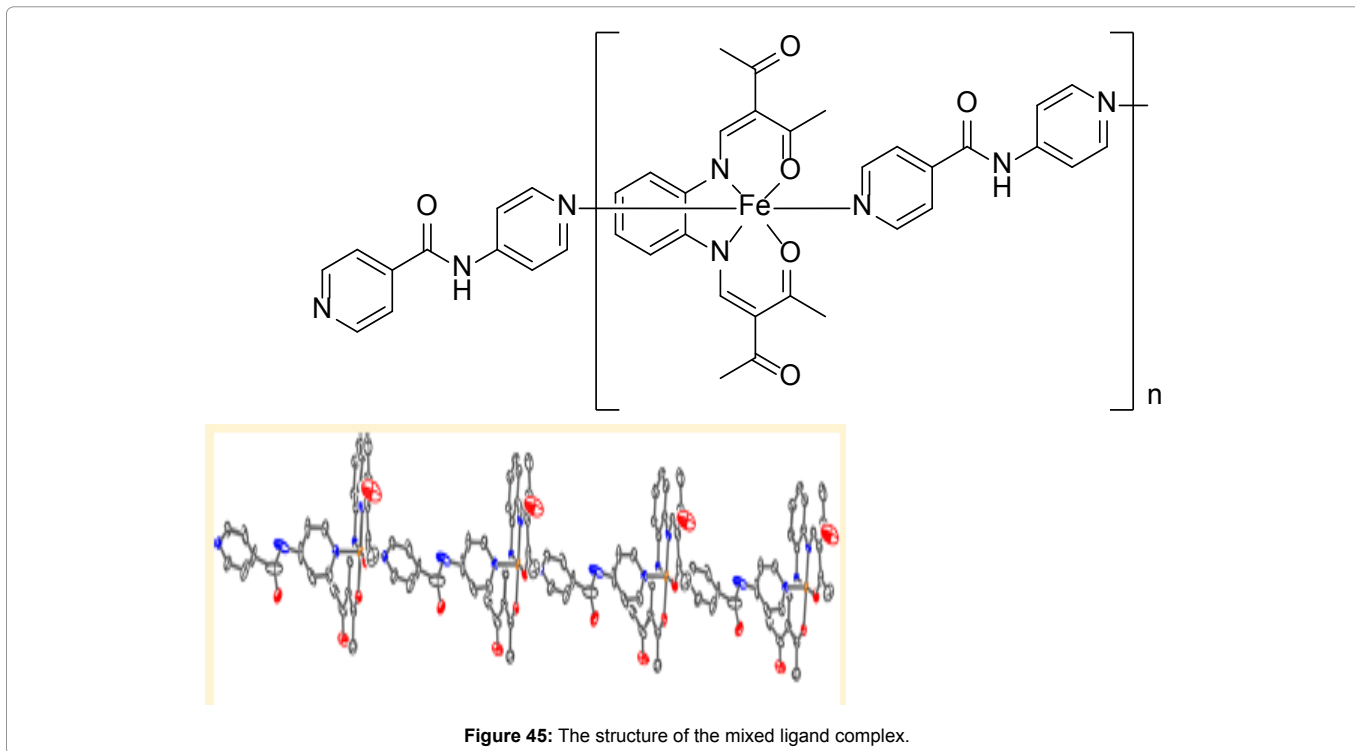
This review describes the state of the art in research about iron ST complexes in relation to their room-temperature switching, a critical criterion for the integration of ST compounds as active components in application devices. The survey showed that there is an increasing number of iron(II) and iron(III) complexes with critical temperatures around room temperature. In general, iron(II) ST complexes exhibit more abrupt transitions  $T_{1/2}$  combined with occasionally very large temperature-induced hysteresis  $\Delta T_{1/2}$ . Coexistence of the latter two ST parameters lead to bistability at ambient conditions, mostly in their solid-state bulk phases. Iron(II) ST complexes also show maximal magnetic discrimination between dia- and paramagnetic

states, while iron(III) ST complexes must deal with two different paramagnetic states (and sometimes even an intermediate spin state). Such a situation complicates the spin-state picture; on the other hand, this class of ST compounds often delivers more pronounced thermochromism.

A common disadvantage of all iron ST systems is that they sometimes show extreme sensitivity to local environmental influences, including crystal packing, inclusion of solvent and anion/cation molecules and concomitant crystalline phase transition events.

Critical switching temperatures at ambient conditions seem to be favored (1) by the use of rigid, multidentate ligand systems. Desirable wide regions of bistability around room temperature can be achieved (2) by multidimensional (1D, 2D, 3D) interlinking of the respective mononuclear ST centers through relatively weak, but multiple hydrogen bonding networks, or stronger coordination bond networks. The use of multinuclear ST compounds does not seem to be useful therein, particularly due to their potential for magnetic exchange processes that dilute the magnetic response and lead to more complex switching schemes.





However, the full process of introducing, integrating, and implementing ST complexes as active units into molecular hybrid devices still has some way to go. The recent reports that persistent ST switching has been observed even in thin nanoscale layers and

particles, are important, since they provide the basis for introducing a ST into a device's architecture. However, spin-state switching in such highly predefined device environments may require — in addition to the previously described triggers of temperature, pressure and light — the development of more suitable triggers, for example the direct application of electrical fields, or the implementation of single-molecule optical readout of the spin state. Addressing single monolayers or even molecules is yet important to be investigated as a research topic. The inherent tendency of ST compounds to respond to multiple triggers simultaneously is a problem, which will probably need to be tackled in the future. However, despite this remaining challenges, the ST phenomenon remains uniquely attractive, equally appealing to chemists, physicists, biologists and electrical engineers, since it leads to new horizons in molecular data processing and storage.

### References

1. Cotton FA, Wilkinson G (1992) *Advanced Inorganic Chemistry*, (3rd edn), Wiley, New York, USA.
2. Ferlay S, Mallah T, Ouahes R, Veillet P, Verdaguer M (1995) A room-temperature organometallic magnet based on Prussian blue. *Nature* 378: 701-703.
3. Kahn O, Martinez CJ (1998) Spin-transition polymers: from molecular materials toward memory devices. *Science* 279: 44-48.
4. Güttlich P, Hauser A, Spiering HC (1994) Thermal and optical switching of Iron(II) complexes. *Angew Chem Int* 33: 2024.
5. Real JA, Gaspar AB, Munoz MC (2005) Thermal, pressure and light switchable spin-crossover materials. *J Chem Soc Dalton Trans* 2062-2079.
6. Niel V, Martinez-Agudo JM, Munoz MC, Gaspar AB, Real JA (2001) Cooperative spin crossover behavior in cyanide-bridged Fe (II)- M (II) bimetallic 3D Hofmann-like networks (M= Ni, Pd, and Pt). *Inorg Chem* 40: 3838-3839.
7. Zaworotko MJ (2000) Nanoporous structures by design. *Angew Chem Int Ed Engl* 39: 3052-3054.

8. Yaghi OM, O'Keeffe M, Ockwig NW, Chae HK, Eddaoudi M, et al. (2003) Reticular synthesis and the design of new materials. *Nature* 423: 705-714.
9. Beauvais LG, Long JR (2002)  $\text{Co}_3[\text{Co}(\text{CN})_5]_2$ , A microspores magnet with an ordering temperature of 38K. *J Am Chem Soc* 124: 12096-12097.
10. Coronado E, Galan-Mascaros JR, Garcia-Gomez CJ, Laukhin V (2000) Coexistence of ferromagnetism and metallic conductivity in a molecule-based layered compound. *Nature* 408: 447-449.
11. Bousseksou A, Molnar G, Demont P, Menegotto (2003) Observation of a thermal hysteresis loop in the dielectric constant of spin crossover complexes: towards molecular memory devices. *J Mater Chem* 13: 2069-2071.
12. Halder GJ, Kepert CJ, Moubaraki B, Murray KS, Cashion JD (2002) Guest-dependent spin crossover in a nanoporous molecular framework materials. *Science* 298: 1762-1765.
13. Madhu NT, Salitros I, Schramm F, Kyatskya S, Fuhr O, et al. (2008) Above room temperature spin transition in a series of iron (II) bis (pyrazolyl) pyridine compounds. *Compt Rend Chimie* 11: 1166-1174.
14. Gütllich P (1981) Spin crossover in iron (II)-complexes. *Struct Bonding* 44: 83-195.
15. Armand F, Badoux C, Bonville P, Ruau-del-Teixier A, Kahn O (1995) Langmuir-blodgett films of spin transition iron (II) metalloorganic polymers. 1. Iron (II) complexes of octadecyl-1, 2, 4-triazole. *Langmuir* 11: 3467-3472.
16. Michalowicz A, Moscovici J, Ducourant B, Cracco D, Kahn O (1995) EXAFS and X-ray powder diffraction studies of the spin transition molecular materials  $[\text{Fe}(\text{Htrz})_2(\text{trz})(\text{BF}_4)]$  and  $[\text{Fe}(\text{Htrz})_3(\text{BF}_4)_2 \cdot \text{H}_2\text{O} (\text{Htrz}= 1, 2, 4\text{-H-triazole}; \text{trz}= 1, 2, 4\text{-triazolato})$ . *Chem Mater* 7: 1833-1842.
17. Kroeber J, Audiere JP, Claude R, Codjovi E, Kahn O, et al. (1994) Spin transitions and thermal hysteresis in the molecular-based materials  $[\text{Fe}(\text{Htrz})_2(\text{trz})(\text{BF}_4)]$  and  $[\text{Fe}(\text{Htrz})_3(\text{BF}_4)_2 \cdot \text{cndot. H}_2\text{O} (\text{Htrz}= 1, 2, 4\text{-H-triazole}; \text{trz}= 1, 2, 4\text{-triazolato})$ . *Chem Mater* 6: 1404-1412.
18. Coronado E, Ramon Galan-Mascaros J, Monrabal-Capilla M, Garcia-Martinez J, Pardo-Ibanez P (2007) Bistable spin-crossover nanoparticles showing magnetic thermal hysteresis near room temperature. *Adv Mater* 19: 1359-1361.
19. Kröber J, Codjovi E, Kahn O, Groliere F, Jay C (1993) A spin transition system with a thermal hysteresis at room temperature. *J Am Chem Soc* 115: 9810-9811.
20. Codjovi E, Sommier L, Kahn O (1996) A spin transition molecular material with an exceptionally large thermal hysteresis loop at room temperature. *New J Chem* 20: 503-505.
21. Cantin C, Daubric H, Kliava J, Servant Y, Sommier L, et al. (1998) Spin transition polymer with a large hysteresis around room temperature: optical response and electron paramagnetic resonance. *J Phys Condens Matter* 10: 7057.
22. van Koningsbruggen PJ, Gracia Y, Codjovi E, Lapouyade R, Kahn O, et al. (1997) Non-classical Fe II spin-crossover behaviour in polymeric iron (II) compounds of formula  $[\text{Fe}(\text{NH}_2\text{trz})_3]_x \cdot x \text{H}_2\text{O} (\text{NH}_2\text{trz}= 4\text{-amino-1, 2, 4-triazole}; X= \text{derivatives of naphthalene sulfonate})$ . *J Mater Chem* 7: 2069-2075.
23. Garcia Y, van Koningsbruggen PJ, Lapouyade R, Rabardel L, Michalowicz A, et al. (1998) Synthesis and spin-crossover characteristics of polynuclear 4-(2'-hydroxy-ethyl)-1, 2, 4-triazole Fe (II) molecular materials. *C R Acad Paris IIC* 1: 523-532.
24. Garcia Y, Guionneau P, Bravic G, Chasseau D, Howard JAK, et al. (2000) Synthesis, crystal structure, magnetic properties and 57Fe Mössbauer spectroscopy of the new trinuclear  $[\text{Fe}_3(4\text{-(2'-hydroxyethyl)-1, 2, 4-triazole})_6(\text{H}_2\text{O})_6](\text{CF}_3\text{SO}_3)_6$  spin crossover compound. *Eur J Inorg Chem* 25: 1531-1538.
25. Schweinfurth D, Demeshko S, Hohloch S, Steinmetz M, Brandenburg JG, et al. (2014) Spin crossover in Fe (II) and Co (II) complexes with the same click-derived tripodal ligand. *Inorg Chem* 53: 8203-8212.
26. Hogue RW, Humphrey L, Feltham C, Miller GR, Brooker S (2016) Spin crossover in dinuclear  $\text{N}_4\text{S}_2$  Iron (II) Thioether-Triazole complexes: Access to [HS-HS], [HS-LS], and [LS-LS] states. *Inorg Chem* 55: 4152-4165.
27. Niel V, Martinez-Agudo JM, Munoz MC, Gaspar AB, Real JA (2001) Cooperative spin crossover behavior in cyanide-bridged Fe (II)- M (II) bimetallic 3D Hofmann-like networks (M= Ni, Pd, and Pt). *Inorg Chem* 40: 3838-3839.
28. Bonhommeau S, Molnar G, Galet A, Zwick A, Real JS, et al. (2005) One Shot Laser Pulse Induced Reversible Spin Transition in the Spin-Crossover Complex  $[\text{Fe}(\text{C}_4\text{H}_4\text{N}_2)(\text{Pt}(\text{CN})_4)]$  at Room Temperature. *Angew Chem Int* 44: 4069-4073.
29. Cobo S, Molnar G, Real JA, Bousseksou A (2006) Multilayer sequential assembly of tin films that display room - temperature spin cross-over with hysteresis. *Angew Chem Int* 45: 5786-5789.
30. Larionova J, Salmon L, Guari Y, Tokarev A, Molvinger K (2008) Towards the ultimate limit of the memory effect in spin cross over solids. *Angew Chem Int* 47: 8236-8240.
31. Munoz MC, Gaspar AB, Galet A, Real JA (2007) Spin-crossover behavior in cyanide-bridged Iron (II)- Silver (I) bimetallic 2D Hofmann-like metal-organic frameworks. *Inorg Chem* 46: 8182-8192.
32. Holland JM, McAllister JA, Kilner CA, Thornton-Pett M, Bridgeman AJ, (2002) Stereochemical effects on the spin-state transition shown by salts of  $[\text{FeL}_2]^{2+} [\text{L}= 2, 6\text{-di}(\text{pyrazol-1-yl})\text{pyridine}]$ . *J Chem Soc Dalton Trans* 548-554.
33. Halcrow MA (2009) Iron(II) complexes of 2,6-di(pyrazol-1-yl)pyridines-A versatile system for spin-crossover research. *Coord Chem Rev* 253: 2493-2514.
34. Halcrow MA (2007) The spin-states and spin-transitions of mononuclear iron (II) complexes of nitrogen-donor ligands. *Polyhedron* 26: 3523-3576.
35. Halcrow MA (2005) The synthesis and coordination chemistry of 2,6-bis (pyrazolyl) pyridines and related ligands-versatile terpyridine analogues. *Coord Chem Rev* 249: 2880-2908.
36. Rajadurai C, Schramm F, Brink S, Fuhr O, Ghafari M, et al. (2006) Spin transition in a chainlike supramolecular iron (II) complex. *Inorg Chem* 45: 10019-10021.
37. Rajadurai C, Schramm F, Fuhr O, Ruben M (2008) An iron (II) spin-transition compound with thiol anchoring groups. *Eur J Inor Chem* 2649-2653.
38. Rajadurai Ch, Fuhr O, Kruk R, Ghafari M, Hahn H, et al. (2007) Above room temperature spin transition in a metallo-supramolecular coordination oligomer/polymer. *Chem Commun* 25: 2636-2638.
39. Clemente-Leon M, Coronado E, Gimenez-Lopez MC, Romero FM (2007) Structural, Thermal, and magnetic study of solvation processes in spin-crossover  $[\text{Fe}(\text{bpp})_2][\text{Cr}(\text{L})(\text{ox})_2]^{2-} \cdot n \text{H}_2\text{O}$  Complexes. *Inorg Chem* 46: 11266-11276.
40. Costa JS, Santiago R, Craig GA, Barth B, Beavers CM, et al. (2014) Three-way crystal-to-crystal reversible transformation and controlled spin switching by a nonporous molecular material. *J Am Chem Soc* 136: 3869-3874.
41. Weber B, Bauer W, Obel J (2008) An iron (II) spin-crossover complex with a 70 K wide thermal hysteresis loop. *Angew Chem Int* 47: 10098-10101.
42. Müller BR, Leibelung B, Jäger BG (2000) Cooperative magnetic behavior of self-assembled iron (II) chelate chain compounds. *Chem Phys Lett* 319: 368-374.
43. Boča R, Baran P, Dilhan L, Fuess H, Haase W, et al. (1997) Crystal structure and spin crossover studies on bis (2,6-bis (benzimidazol-2-yl) pyridine) iron (II) perchlorate. *Inorg Chim Acta* 260: 129-136.
44. Boča R, Boča M, Dilhan L, Falk K, Fuess H, et al. (2001) Strong cooperativeness in the mononuclear iron (II) derivative exhibiting an abrupt spin transition above 400 K. *Inorg Chem* 40: 3025-3033.
45. Boča R, Renz F, Boča M, Fuess H, Haase W, et al. (2005) Tuning the spin crossover above room temperature: iron (II) complexes of substituted and deprotonated 2, 6-bis (benzimidazol-2-yl) pyridine. *Inorg Chem Comm* 8: 227-230.
46. Boča R, Baran P, Boča M, Dilhan L, Fuess H, et al. Spin crossover in bis (2,6-bis (benzimidazol-2-yl) pyridine) iron (II) tetraphenylborate. *Inorg Chim Acta* 278: 190-196.
47. Sams JR, Tsin TB (1976) 5T<sub>2g</sub>-1A<sub>1g</sub> Spin crossover in tris [2-(2'-pyridyl) benzimidazole] iron (II) complexes. *Inorg Chem* 15: 1544-1550.
48. König E, Ritter G, Kulshreshtha SK, Waigler J, Goodwin HA (1984) The discontinuous high-spin (5T<sub>2</sub>) d<sub>5</sub>high-spin (1A<sub>1</sub>) transition in solid bis (1, 10-phenanthroline-2-carbaldehyde phenylhydrazone) iron (II) bis (tetrafluoroborate): hysteresis effects, concurrent crystallographic phase change, entropy of the transition, and effect of pressure. *Inorg Chem* 23: 1896-1902.

49. König E, Kanellakopulos B, Powietzka B, Goodwin HA (1990) Detailed hysteresis studies and nature of the spin-state transition in bis (1, 10-phenanthroline-2-carbaldehyde phenylhydrazone) iron (II) complexes. *Inorg Chem* 29: 4944-4949.
50. König E, Ritter G, Waigler J, Goodwin HA (1985) The effect of pressure on the thermal hysteresis of the first-order spin transition in bis (1, 10-phenanthroline-2-carbaldehyde phenylhydrazone) iron (II) complexes. *J Chem Phys* 83: 3055-3061.
51. Thiel A, Bousseksou A, Verelst M, Varret F, Tuchagues JP (1999) Dynamic spin-crossover in [Fe II (TRIM)<sub>2</sub>] Br<sub>2</sub> and [Fe II (TRIM)<sub>2</sub>](HCO<sub>2</sub>)<sub>2</sub> investigated by Mössbauer spectroscopy and magnetic measurements. *Chem Phys Lett* 302: 549-554.
52. Min KS, DiPasquale A, Arnold L, Rheingold AL, Miller JS (2007) Room-temperature spin crossover observed for [(TPyA) FeII (DBQ2-)] FeII (TPyA)] 2+[TPyA= Tris (2-pyridylmethyl) amine; DBQ2-= 2, 5-Di-tert-butyl-3, 6-dihydroxy-1, 4-benzoquinone]. *Inorg Chem* 46: 1048-1050.
53. Iasco O, Riviere E, Guillot R, Buron-Le Coinle M, Meunier JF, et al. (2015) Fe<sup>II</sup> (pap-5NO<sub>2</sub>)<sub>2</sub> and Fe<sup>II</sup> (qsal-5NO<sub>2</sub>)<sub>2</sub> Schiff base spin crossover complexes: A rare example with photomagnetism and room-temperature bistability. *Inorg Chem* 54: 1791-1799.
54. Huang W, Shen F, Zhang M, Wu D, Pan F, et al. (2016) Room-temperature switching of magnetic hysteresis by reversible single-crystal-to-single-crystal solvent exchange in imidazole- inspired Fe(II) complexes. *Dalton Trans* 45: 14911-14918.
55. Qin LF, Pang CY, Han WK, Zhang FL, Tian L, et al. (2016) Spin crossover properties of enantiomers, co-enantiomers, racemates, and co-racemates. *Dalton Trans* 45: 7340.
56. Lochenie C, Bauer W, Railliet AP, Schlamp S, Garcia Y, et al. (2014) Large thermal hysteresis for iron(II) spin crossover with N-(Pyrid-4-yl) isonicotinamide. *Inorg Chem* 53: 11563.

### Author Affiliation

Top

<sup>1</sup>Department of Chemistry, Addis Ababa Science and Technology University, Addis Ababa, P.O.Box.16417, Ethiopia

<sup>2</sup>Department of Chemistry, University of Hawassa, Sidama, P. O. Box.05, Ethiopia

<sup>3</sup>Department of Chemistry, Adama Science and Technology University, Adama, P. O. Box. 1888, Ethiopia

<sup>4</sup>Institute of Applied Synthetic Chemistry, Vienna University of Technology, Getreidemarkt 9/163-AC, A-1060 Vienna, Austria

### Submit your next manuscript and get advantages of SciTechnol submissions

- ❖ 80 Journals
- ❖ 21 Day rapid review process
- ❖ 3000 Editorial team
- ❖ 5 Million readers
- ❖ More than 5000 
- ❖ Quality and quick review processing through Editorial Manager System

Submit your next manuscript at • [www.scitechnol.com/submission](http://www.scitechnol.com/submission)